Supporting Information

for

Towards universal stimuli-responsive Drug Delivery Systems based on the tetrazole-containing polymers: synthesis of pillar[5]arenes and their self-assembly into nanocontainers

Dmitriy N. Shurpik, [1] Lyaysan I. Makhmutova, [1] Konstantin S. Usachev, [2] Daut R. Islamov, [3] Olga A. Mostovaya, [1] Anastasia A. Nazarova, [1] Valeriy N. Kizhnyaev [4] and Ivan I. Stoikov [1,*]

[1] Kazan Federal University, A.M. Butlerov Chemical Institute, 420008 Kremlevskaya, 18, Kazan, Russian Federation

[2] Kazan Federal University, Institute of Fundamental Medicine and Biology, 420008 Kremlevskaya, 18, Kazan, Russian Federation

[3] Russian Academy of Sciences, Arbuzov Institute of Organic and Physical Chemistry, FRC Kazan Scientific Center, 420088, Arbuzov st., 8, Kazan, Russian Federation

[4] Irkutsk State University, 664003 K. Marksa, 1, Irkutsk, Russian Federation

E-mail: Ivan.Stoikov@mail.ru

* Corresponding author. Tel.: +7-8432-337463; fax: +7-8432-752253; e-mail: Ivan.Stoikov@mail.ru

Table of contents

1. NMR, MALDI TOF MS, IR spectra of the compounds 6-12

Figure S1. ^{1}H NMR spectrum of 4,8,14,18,23,26,28,31,32,35-deca-(4-methylbenzylsulfonate-1-ethoxy)-pillar[5]arene (**6**), $CDCl_3$, 298 K, 400 MHz.

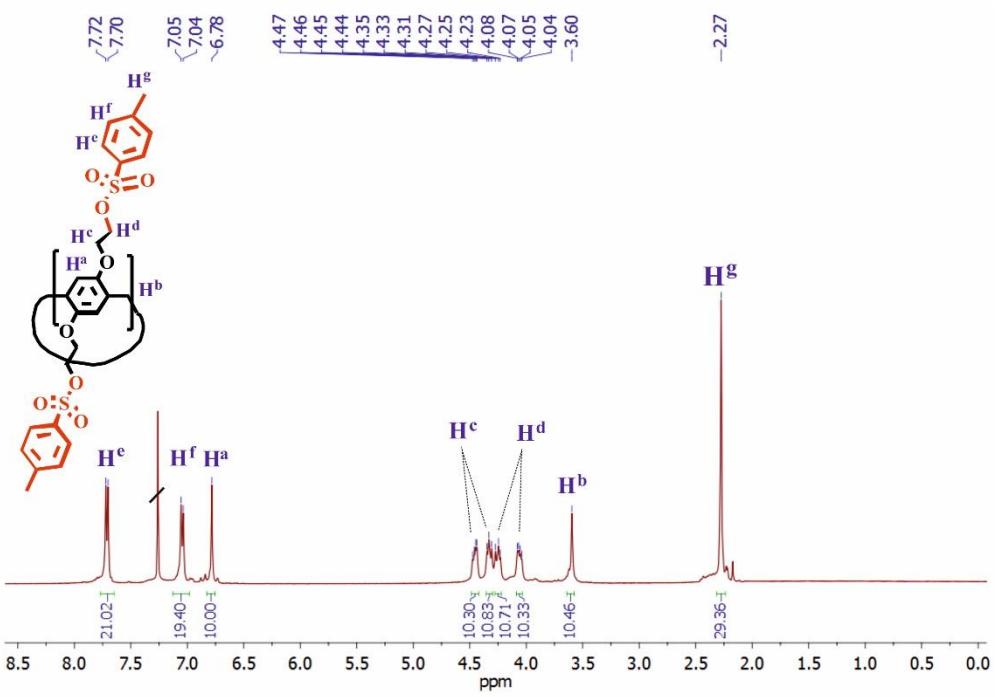

Figure S2. ^{13}C NMR spectrum of 4,8,14,18,23,26,28,31,32,35-deca-(4-methylbenzylsulfonate-1-ethoxy)-pillar[5]arene (**6**), $CDCl_3$, 298 K, 100 MHz.

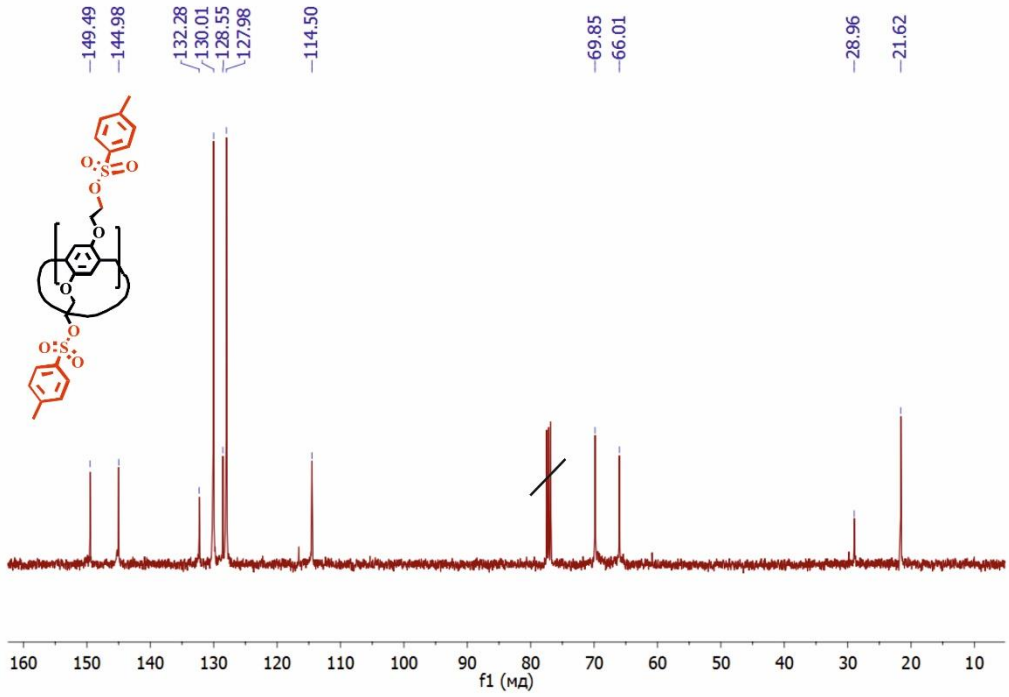

Figure S3. Mass spectrum (MALDI-TOF, 4-nitroaniline matrix) of 4,8,14,18,23,26,28,31,32,35-deca-(4-methylbenzylsulfonate-1-ethoxy)-pillar[5]arene (**6**).

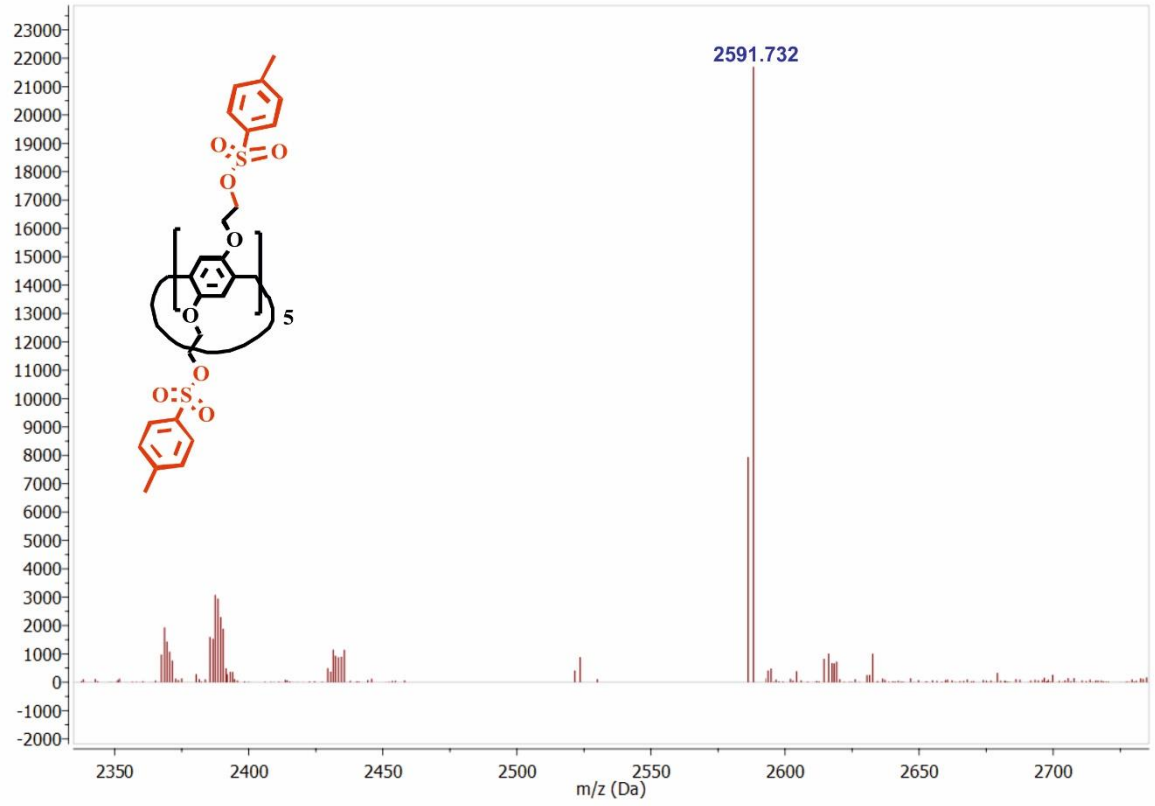

Figure S4. IR spectrum of 4,8,14,18,23,26,28,31,32,35-deca-(4-methylbenzylsulfonate-1-ethoxy)-pillar[5]arene (**6**).

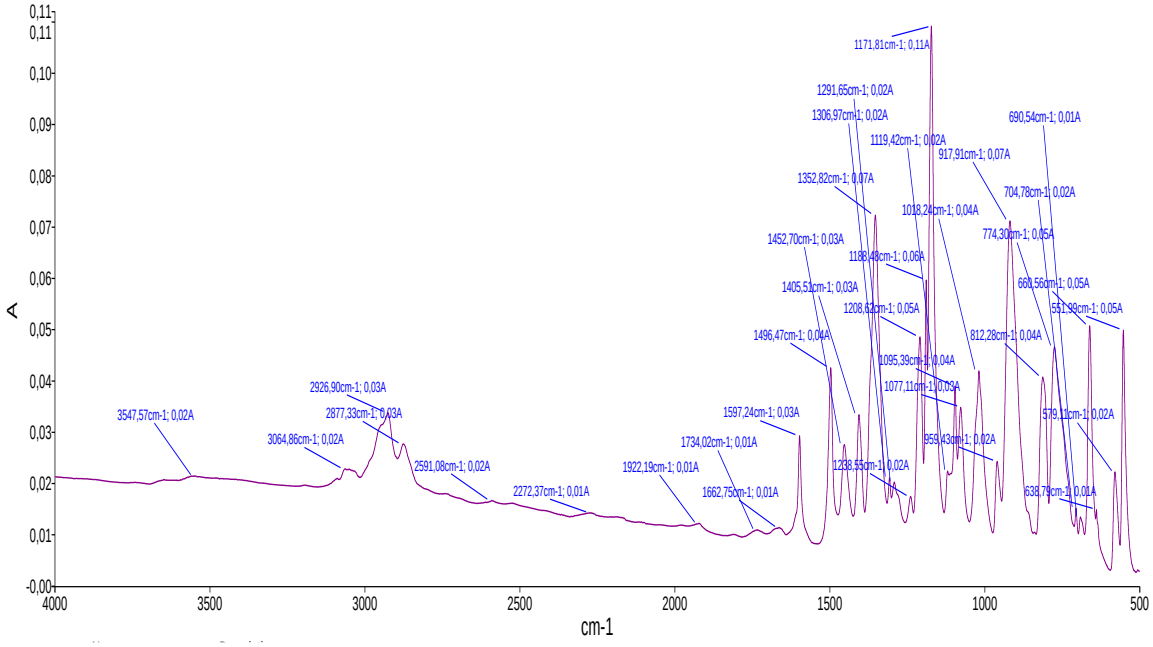

Figure S5. ^{1}H NMR spectrum of 4,8,14,18,23,26,28,31,32,35-deca-[(isoindoline-1,3-dione)propoxy]-pillar[5]arene (**11**), $CDCl_3$, 298 K, 400 MHz.

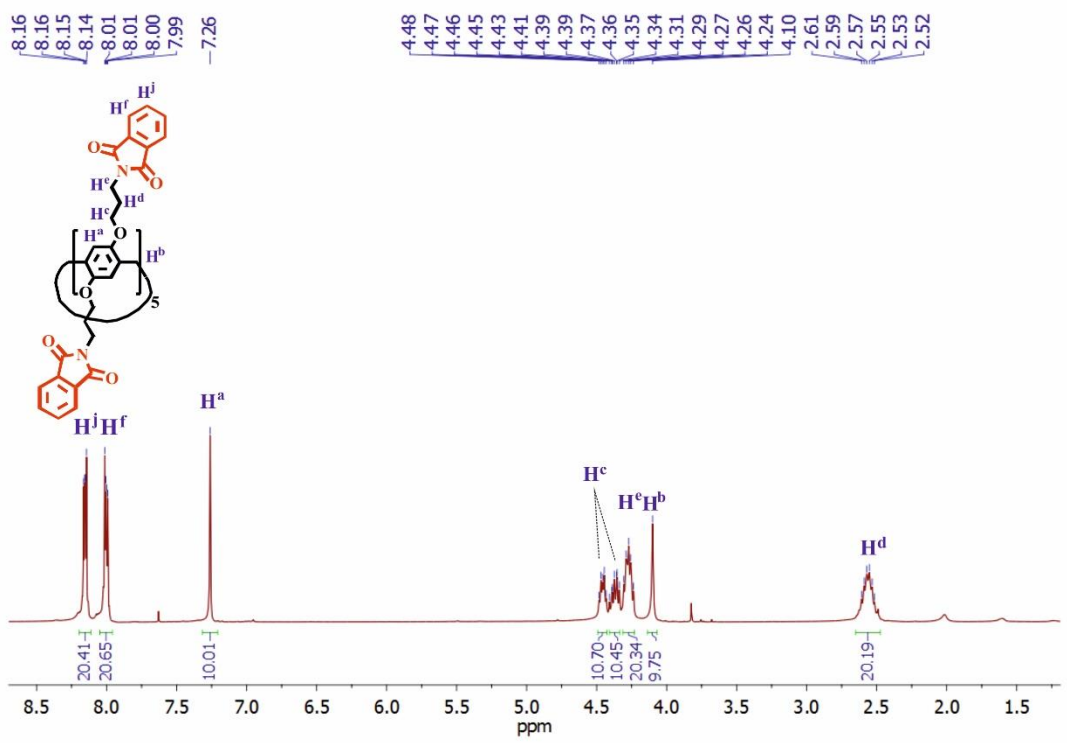

Figure S6. ^{13}C NMR spectrum of 4,8,14,18,23,26,28,31,32,35-deca-[(isoindoline-1,3-dione)propoxy]-pillar[5]arene (**11**), $CDCl_3$, 298 K, 100 MHz.

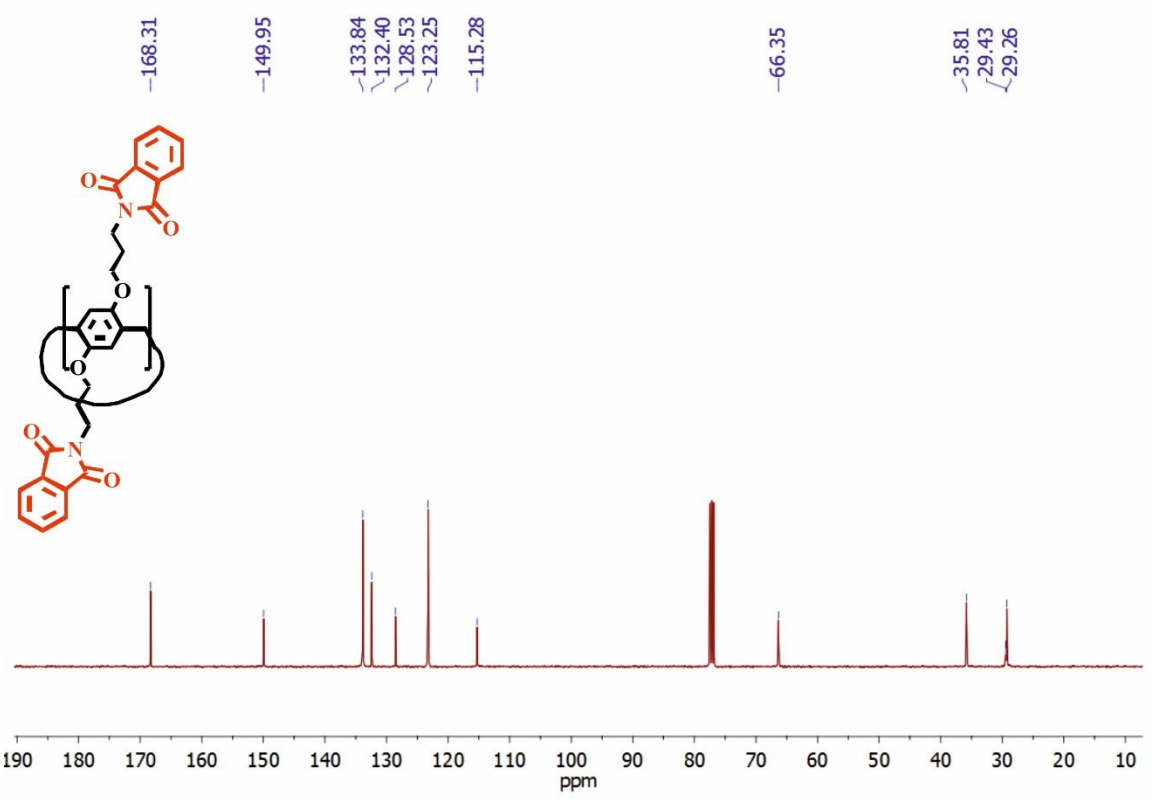

Figure S7. IR spectrum of 4,8,14,18,23,26,28,31,32,35-deca-[(isoindoline-1,3-dione)propoxy]-pillar[5]arene (**11**).

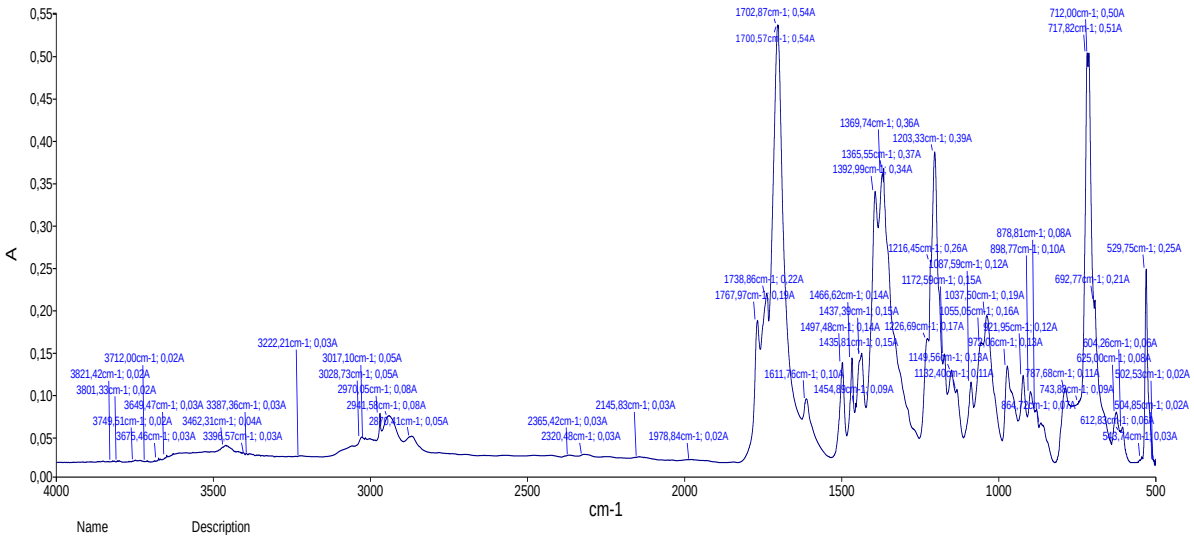

Figure S8. Mass spectrum (MALDI-TOF, 4-nitroaniline matrix) of 4,8,14,18,23,26,28,31,32,35-deca-[(isoindoline-1,3-dione)propoxy]-pillar[5]arene (**11**)

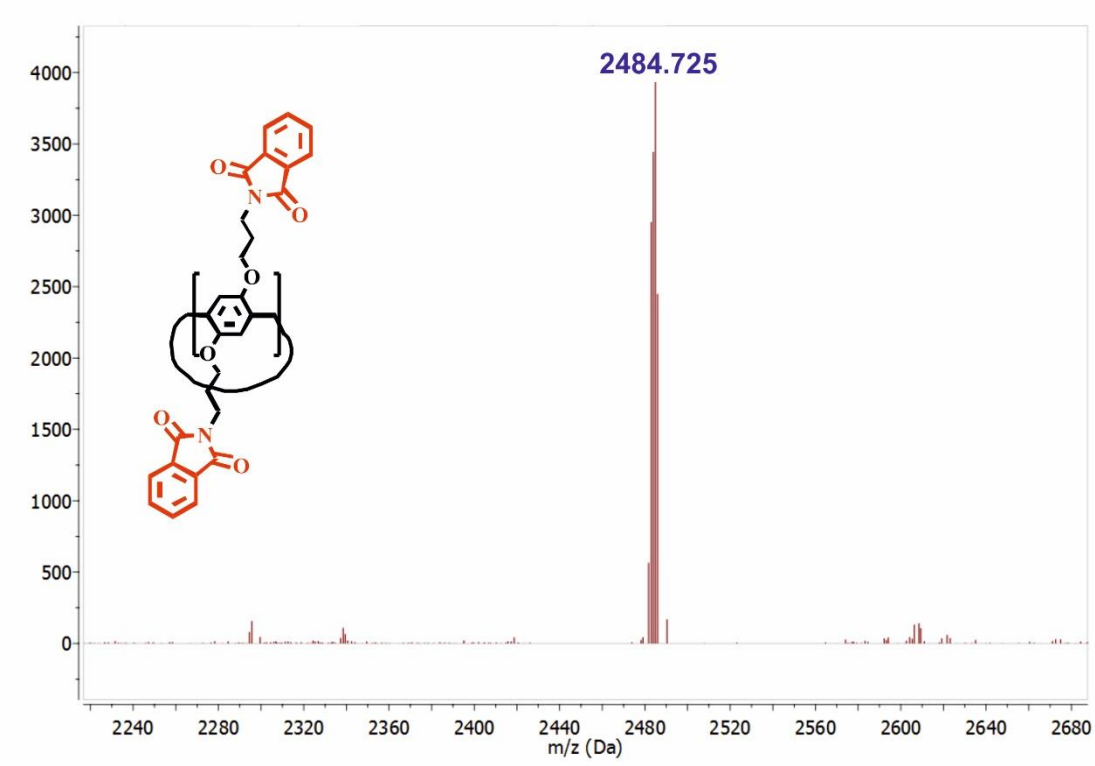

Figure S9. ^{1}H NMR spectrum of 4,8,14,18,23,26,28,31,32,35-deca-[2-(pyrrolidin-1-yl)ethoxy]-pillar[5]arene (7), $CDCl_3$, 298 K, 400 MHz.

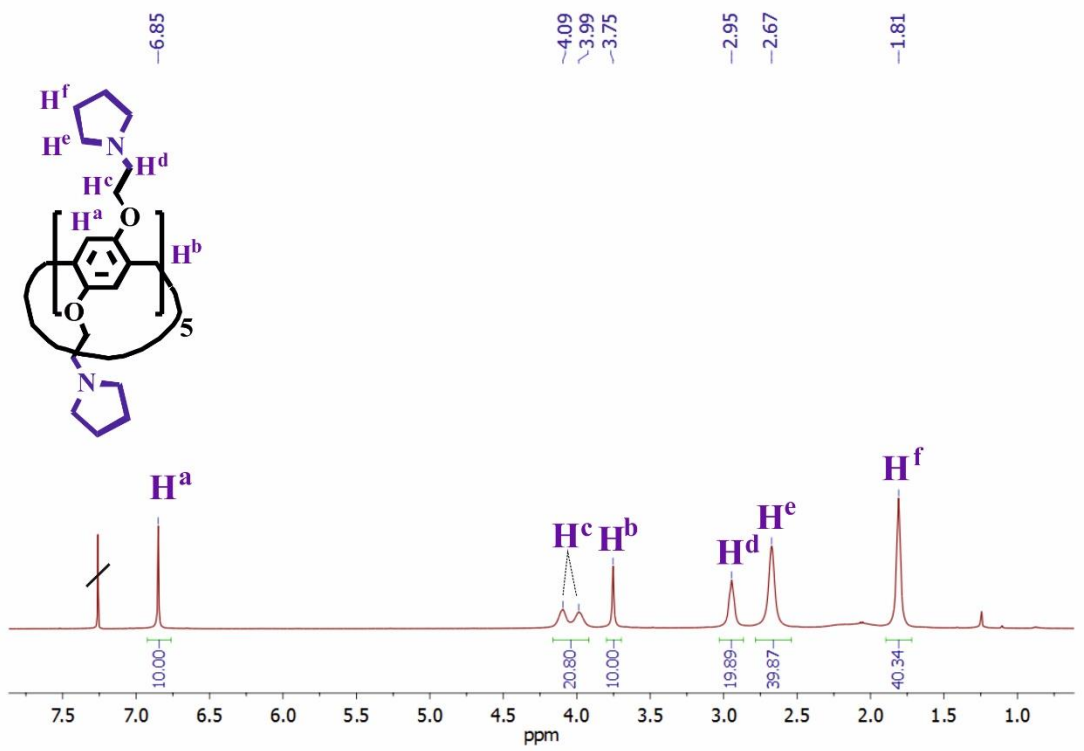

Figure S10. ^{13}C NMR spectrum of 4,8,14,18,23,26,28,31,32,35-deca-[2-(pyrrolidin-1-yl)ethoxy]-pillar[5]arene (**7**), $CDCl_3$, 298 K, 100 MHz.

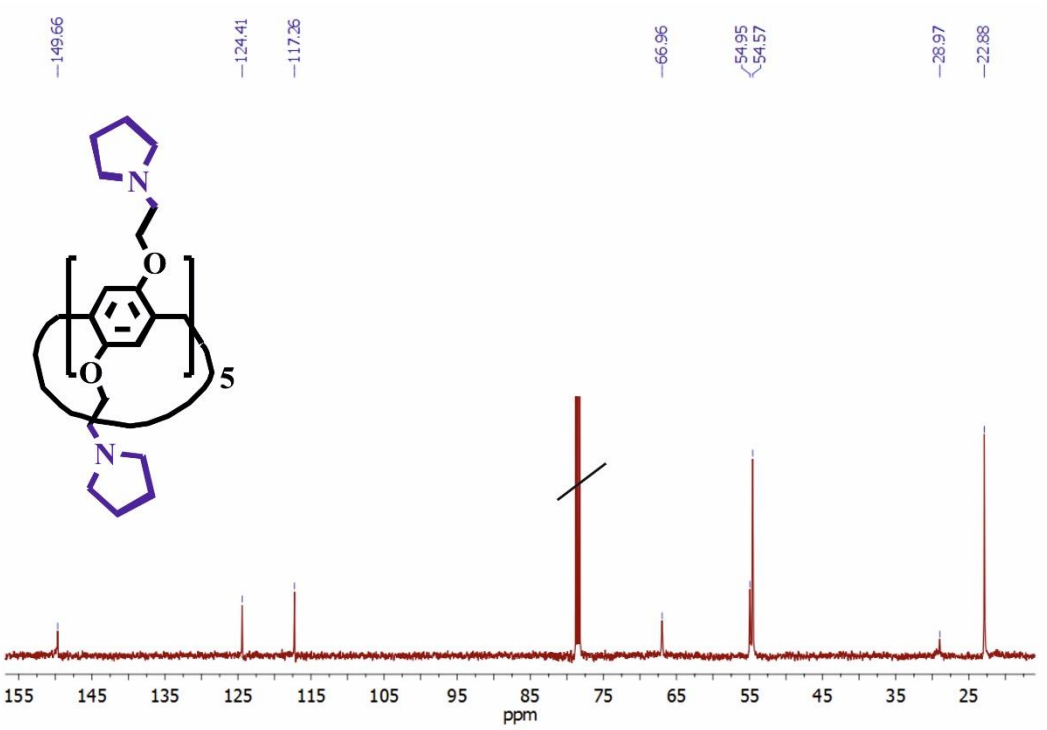

Figure S11. Mass spectrum (MALDI-TOF, 4-nitroaniline matrix) of 4,8,14,18,23,26,28,31,32,35-deca-[2-(pyrrolidin-1-yl)ethoxy]-pillar[5]arene (**7**).

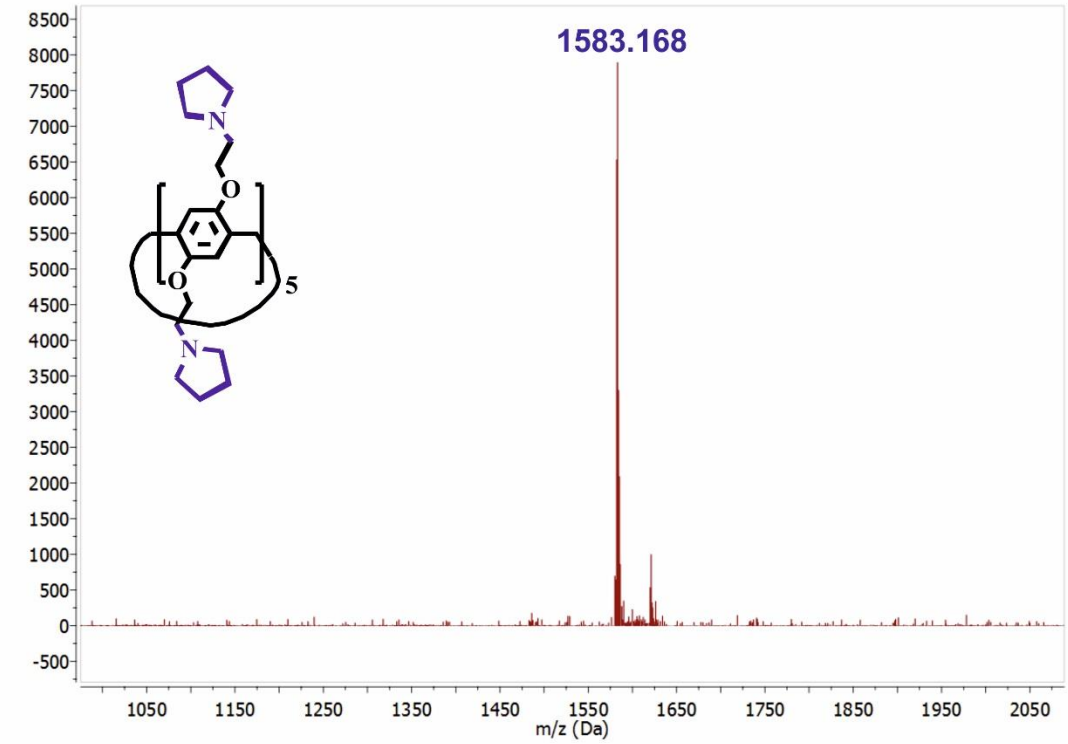

Figure S12. IR spectrum of 4,8,14,18,23,26,28,31,32,35-deca-[2-(pyrrolidin-1-yl)ethoxy]-pillar[5]arene (**7**).

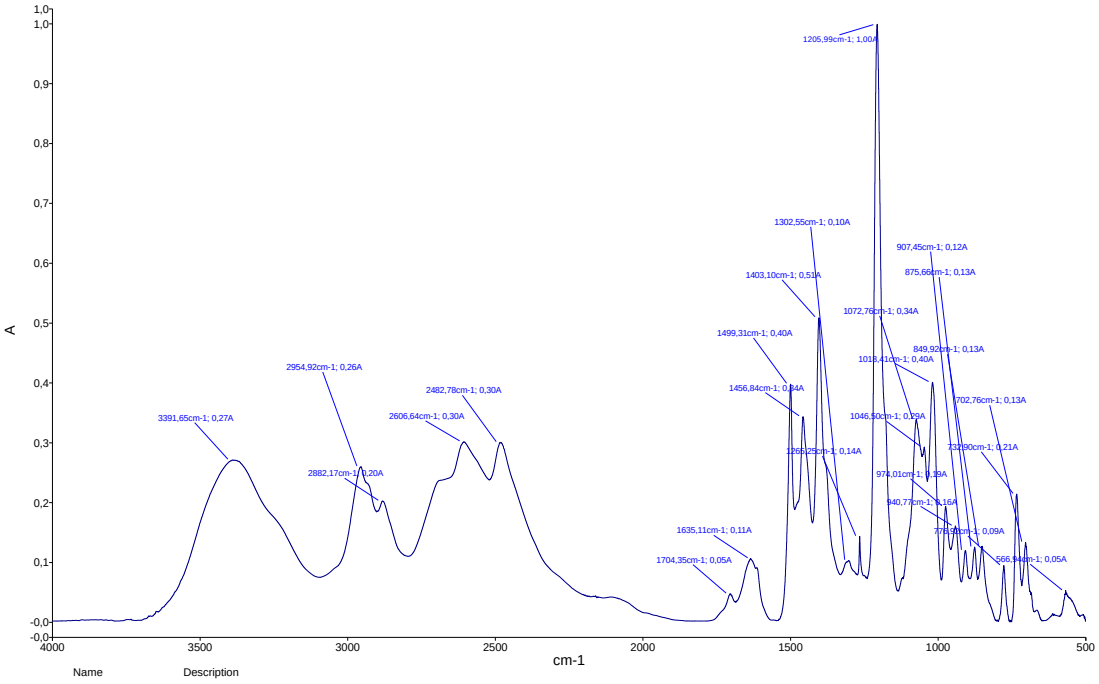

Figure S13. ^{1}H NMR spectrum of 4,8,14,18,23,26,28,31,32,35-deca-[2-(piperidin-1-yl)ethoxy]-pillar[5]arene (**8**) , $CDCl_3$, 298 K, 400 MHz.

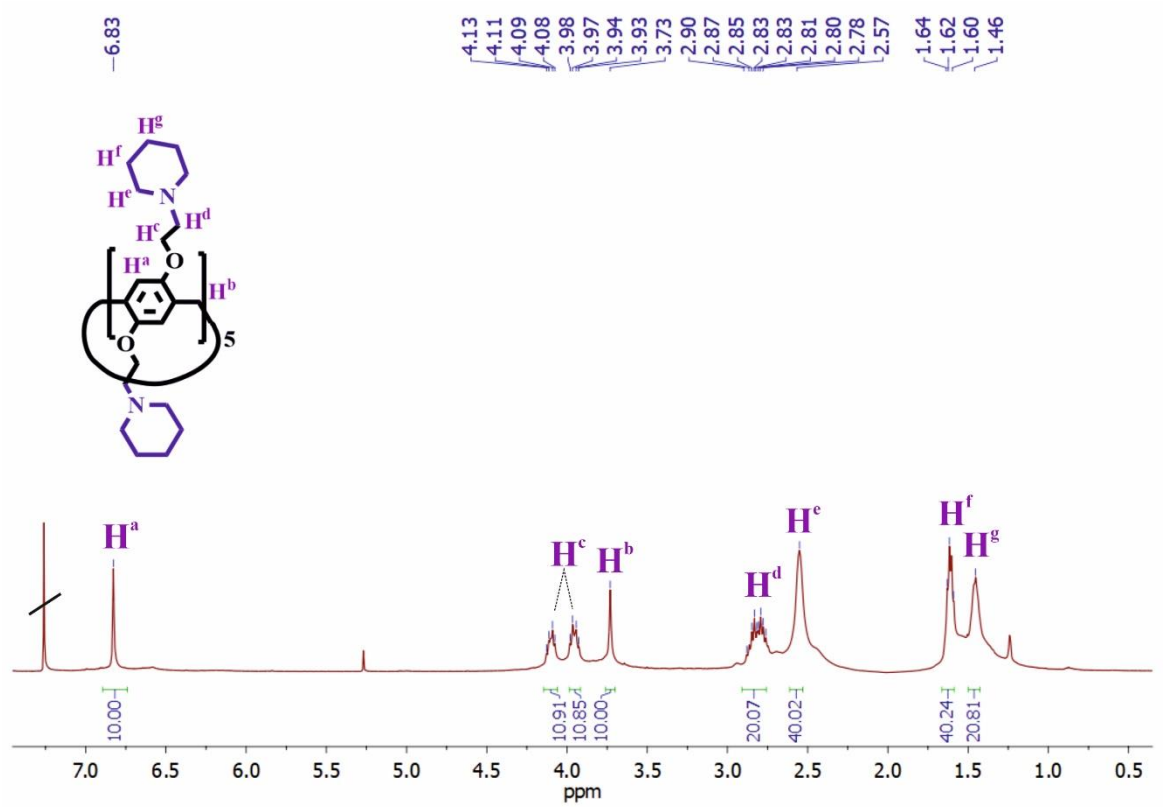

Figure S14. ^{13}C NMR spectrum of 4,8,14,18,23,26,28,31,32,35-deca-[2-(piperidin-1-yl)ethoxy]-pillar[5]arene (**8**), $CDCl_3$, 298 K, 100 MHz.

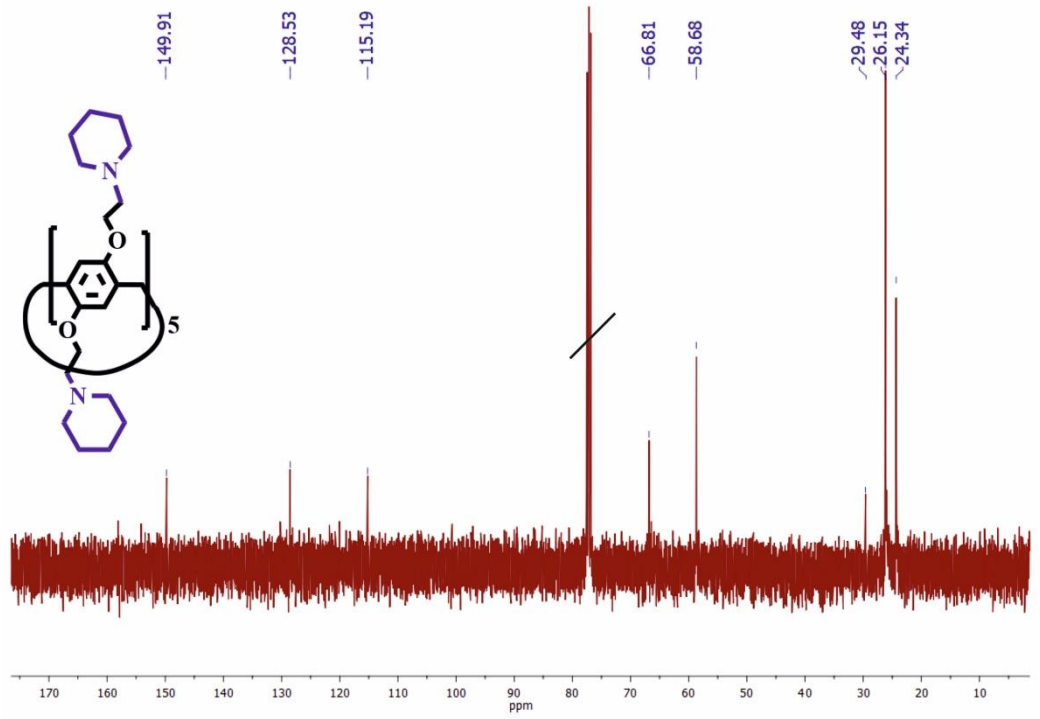

Figure S15. Mass spectrum (MALDI-TOF, 4-nitroaniline matrix) of 4,8,14,18,23,26,28,31,32,35-deca-[2-(piperidin-1-yl)ethoxy]-pillar[5]arene (**8**).

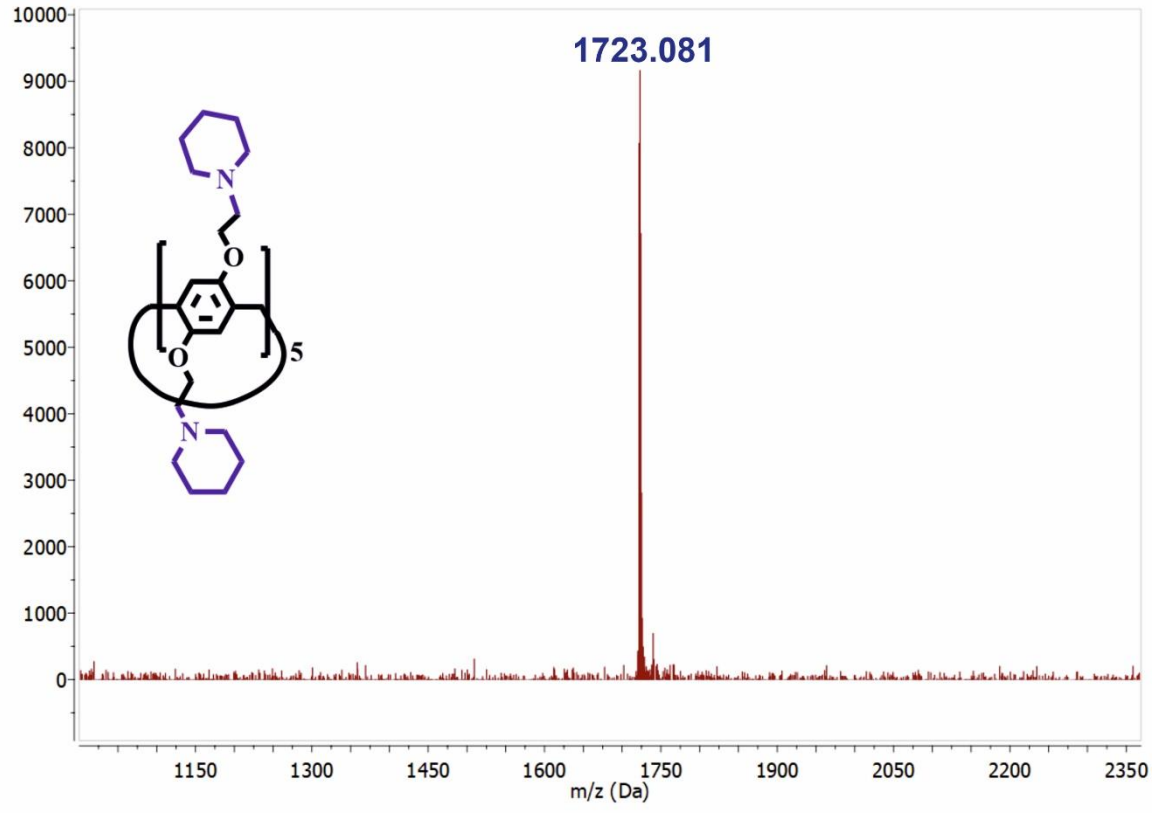

Figure S16. IR spectrum of 4,8,14,18,23,26,28,31,32,35-deca-[2-(piperidin-1-yl)ethoxy]-pillar[5]arene (**8**).

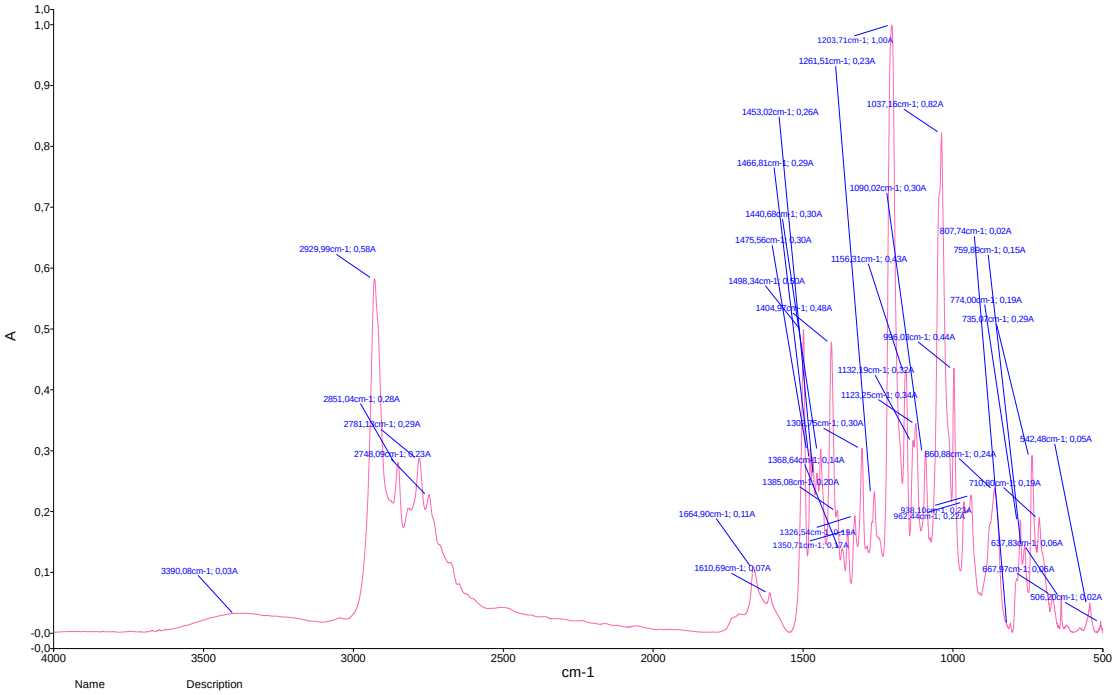

Figure S17. ^{1}H NMR spectrum of 4,8,14,18,23,26,28,31,32,35-deca-(2-morpholinoethoxy)-pillar[5]arene (**9**), $CDCl_3$, 298 K, 400 MHz.

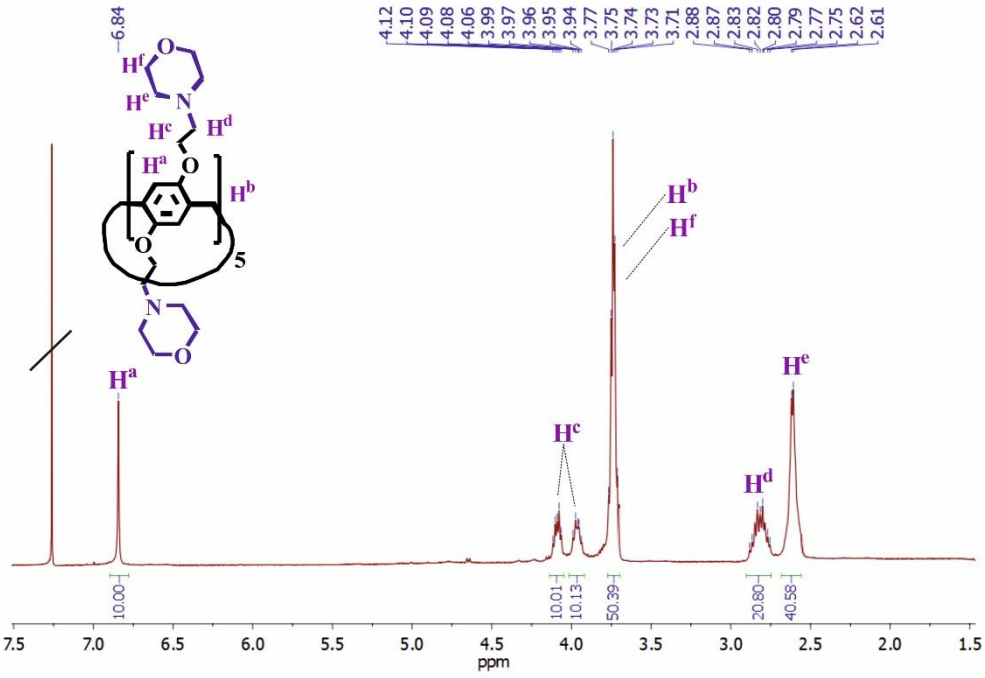

Figure S18. ^{13}C NMR spectrum of 4,8,14,18,23,26,28,31,32,35-deca-(2-morpholinoethoxy)-pillar[5]arene (**9**), $CDCl_3$, 298 K, 100 MHz.

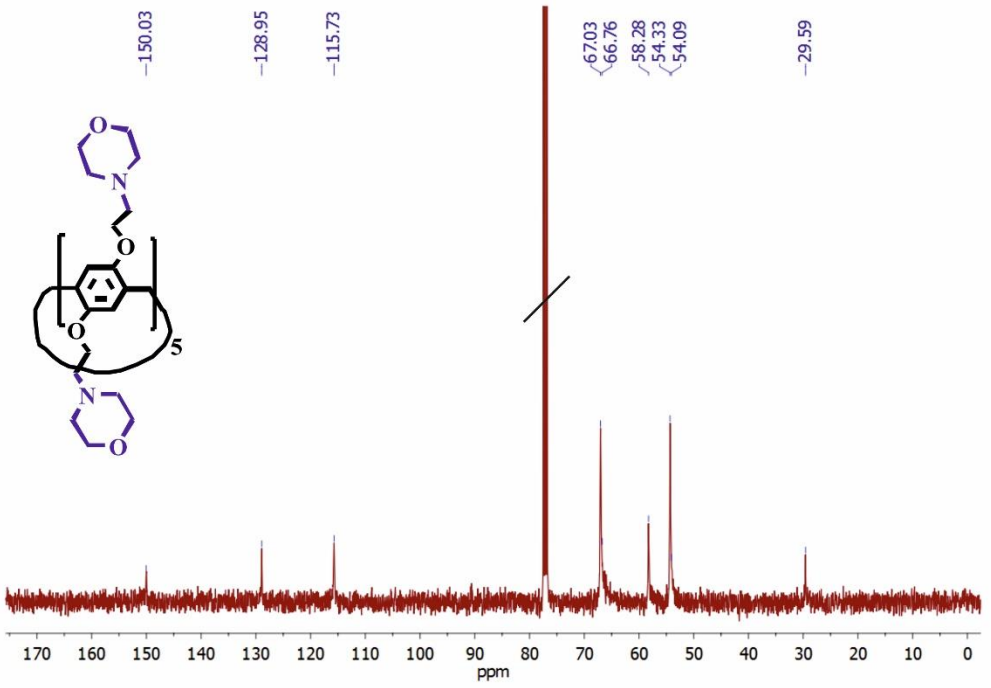

Figure S19. Mass spectrum (MALDI-TOF, 4-nitroaniline matrix) of 4,8,14,18,23,26,28,31,32,35-deca-(2-morpholinoethoxy)-pillar[5]arene (**9**).

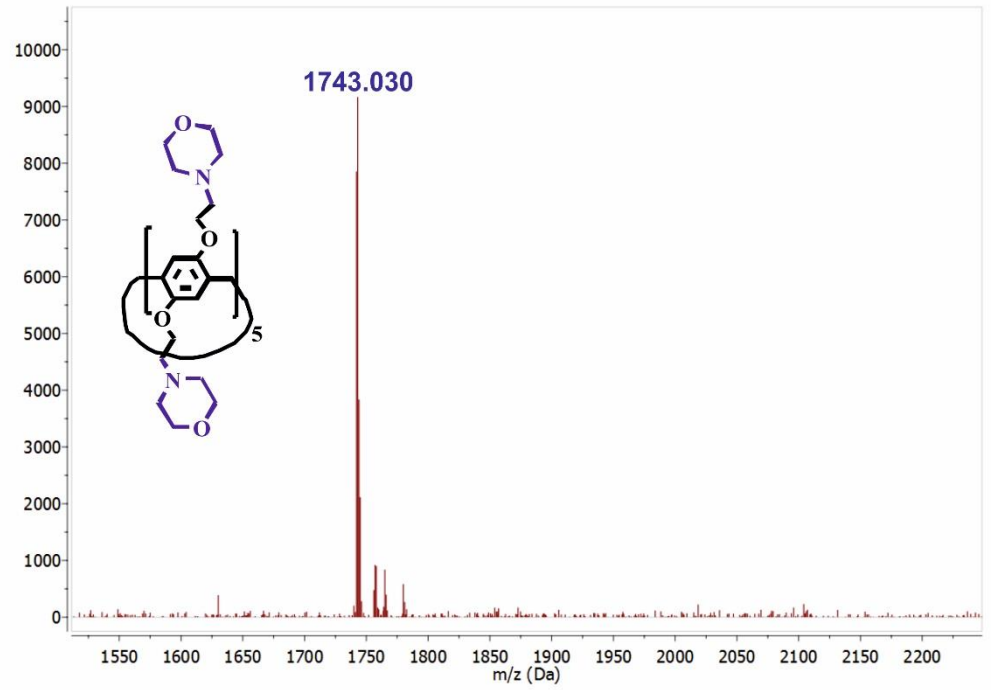

Figure S20. IR spectrum of 4,8,14,18,23,26,28,31,32,35-deca-(2-morpholinoethoxy)-pillar[5]arene (**9**).

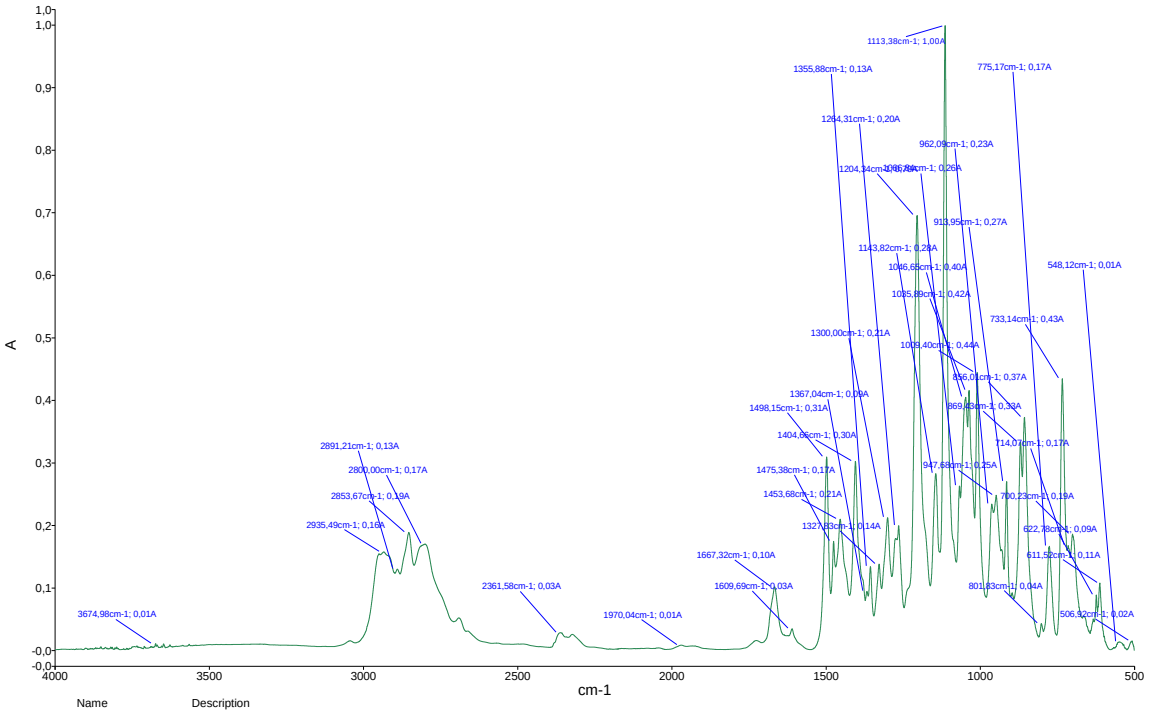

Figure S21. ^{1}H NMR spectrum of 4,8,14,18,23,26,28,31,32,35-deca-(aminopropyloxy)-pillar[5]arene (**12**), D_2O, 298 K, 400 MHz.

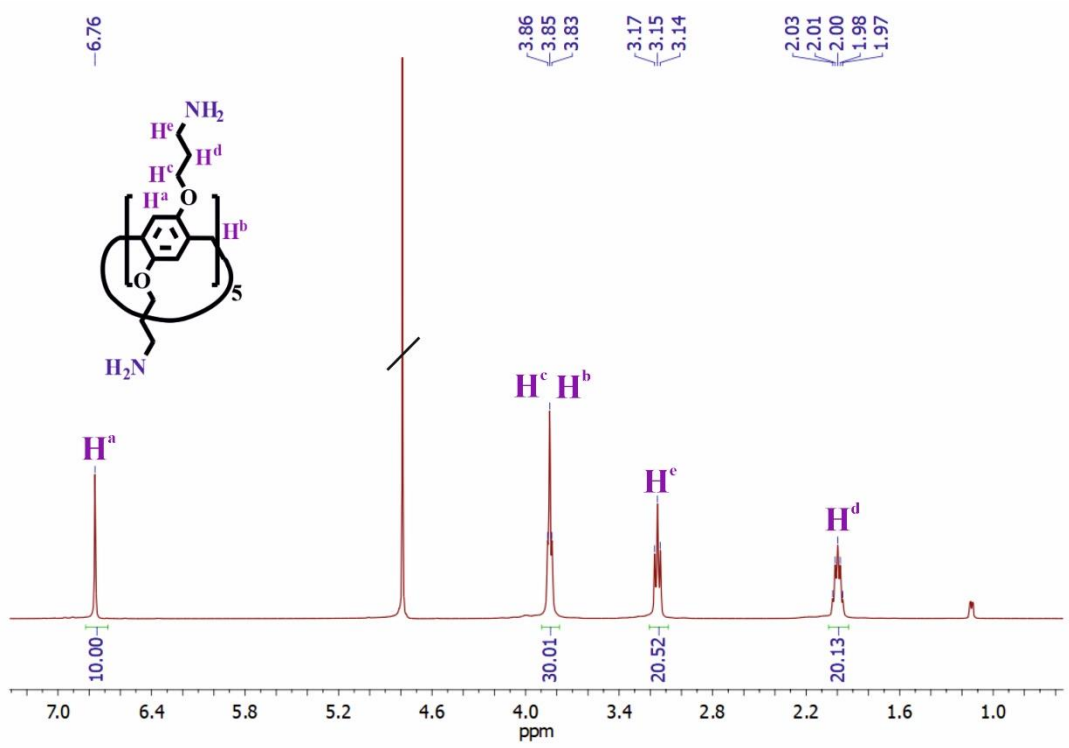

Figure S22.^{13}C NMR spectrum of 4,8,14,18,23,26,28,31,32,35-deca-(aminopropyloxy)-pillar[5]arene (12), D_2O, 298 K, 100 MHz.

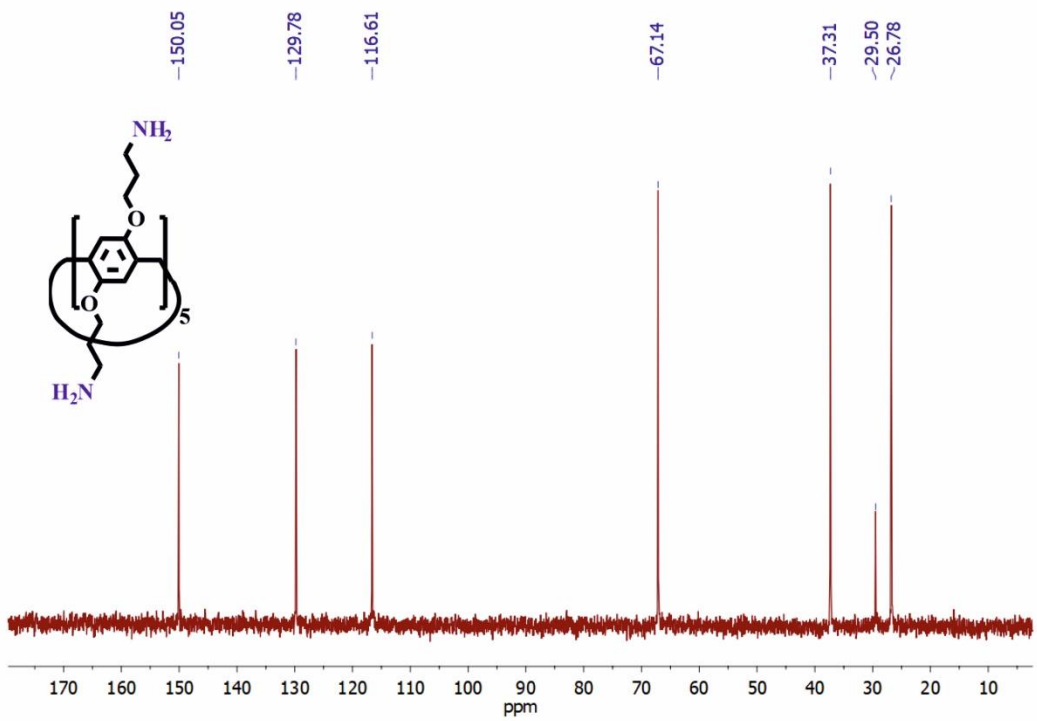

Figure S23. Mass spectrum (MALDI-TOF, 4-nitroaniline matrix) of 4,8,14,18,23,26,28,31,32,35-deca-(aminopropyloxy)-pillar[5]arene (**12**).

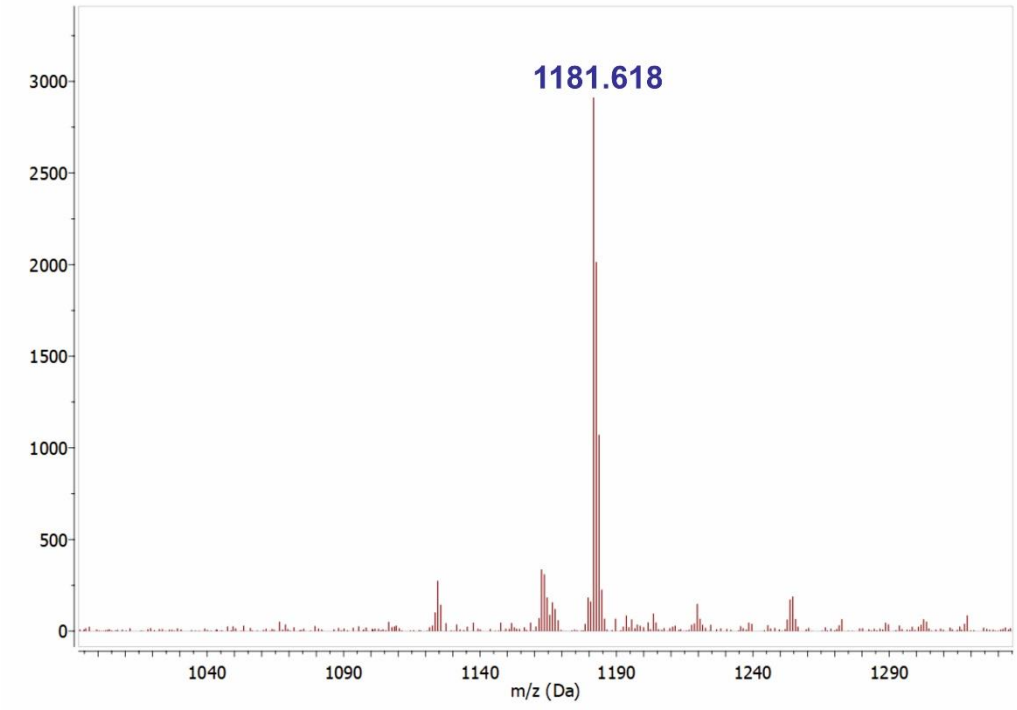

Figure S24. IR spectrum of 4,8,14,18,23,26,28,31,32,35-deca-(aminopropyloxy)-pillar[5]arene (**12**).

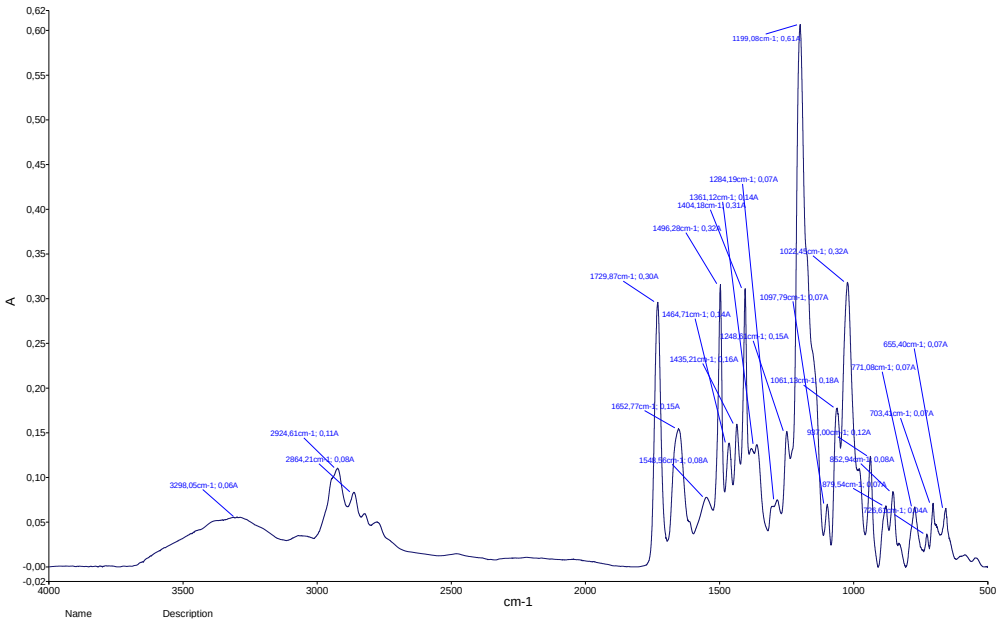

Figure S25. ^{1}H-^{13}C HSQC NMR spectrum of 4,8,14,18,23,26,28,31,32,35-deca-(4-methylbenzylsulfonate-1-ethoxy)-pillar[5]arene (6), $CDCl_3$, 298 K, 400 MHz.

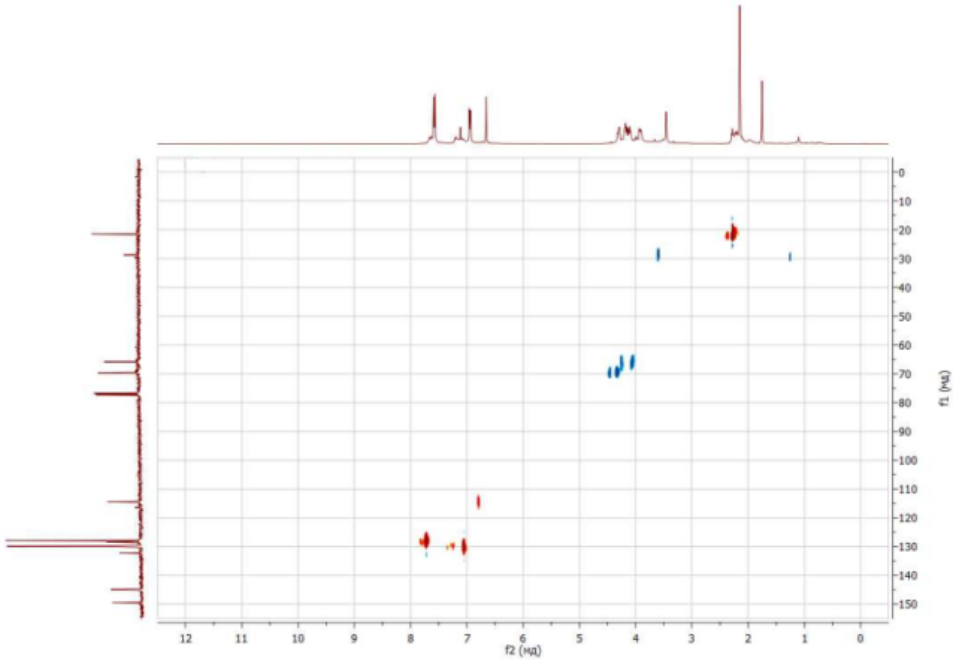

Table S1. Reaction conditions for the synthesis of target macrocycles **6** and **11** from starting compounds **5** and **10**, respectively.

Conditions	Compounds (equiv.)			Solvent	Temp. (°C)	Time (h)	Yield (%)
	Starting compound	Methylene Bridge reagent	Catalyst				
1	**5** (1 equiv.)	PFA (3 equiv.)	$BF_3 \times Et_2O$ (1 equiv.)	$CH_2Cl\text{-}CH_2Cl$	0-85	0.5-24	40-64
2	**5** (1 equiv.)	PFA (3 equiv.)	$BF_3 \times Et_2O$ (1 equiv.)	$CHCl_3$	0-50	2-24	5-20[1]
3	**5** (1 equiv.)	PFA (3 equiv.)	$BF_3 \times Et_2O$ (1 equiv.)	CH_2Cl_2	0-30	2-24	0
4	**5** (1 equiv.)	PFA (3 equiv.)	$AlBr_3$ (1 equiv.)	$CH_2Cl\text{-}CH_2Cl$	0-85	0.5-24	2-25
5	**5** (1 equiv.)	PFA (3 equiv.)	$AlBr_3$ (1 equiv.)	$CHCl_3$	0-50	2-24	4-40[1]
6	**5** (1 equiv.)	PFA (3 equiv.)	$AlBr_3$ (1 equiv.)	CH_2Cl_2	0-30	2-24	0
7	**5** (1 equiv.)	PFA (3 equiv.)	CF_3SO_3H (1 equiv.)	$CH_2Cl\text{-}CH_2Cl$	0-85	0.5-5	35-85
8	**5**	PFA	CF_3SO_3H	$CHCl_3$	0-50	0.5-5	7-45[1]

	(1 equiv.)	(3 equiv.)	(1 equiv.)				
9	**5** (1 equiv.)	PFA (3 equiv.)	CF_3SO_3H (1 equiv.)	CH_2Cl_2	0-30	0.5-5	0
10	**5** (1 equiv.)	PFA (3 equiv.)	CF_3COOH (1 equiv.)	CH_2Cl-CH_2Cl	0-85	0.5-5	1-10
11	**5** (1 equiv.)	PFA (3 equiv.)	CF_3COOH (1 equiv.)	$CHCl_3$	0-50	2-24	1-15[1]
12	**5** (1 equiv.)	PFA (3 equiv.)	CF_3COOH (1 equiv.)	CH_2Cl_2	0-30	2-24	0
13	**5** (1 equiv.)	Paraldehyde (3 equiv.)	$BF_3 \times Et_2O$ (1 equiv.)	CH_2Cl-CH_2Cl	0-85	0.5-24	5-16
14	**5** (1 equiv.)	Paraldehyde (3 equiv.)	CF_3SO_3H (1 equiv.)	CH_2Cl-CH_2Cl	0-85	0.5-24	10-20
15	**10** (1 equiv.)	PFA (3 equiv.)	$BF_3 \times Et_2O$ (1 equiv.)	CH_2Cl-CH_2Cl	0-85	0.5-24	21-53
16	**10** (1 equiv.)	PFA (3 equiv.)	$BF_3 \times Et_2O$ (1 equiv.)	$CHCl_3$	0-50	2-24	1-15[1]
17	**10** (1 equiv.)	PFA (3 equiv.)	$BF_3 \times Et_2O$ (1 equiv.)	CH_2Cl_2	0-30	2-24	0
18	**10** (1 equiv.)	PFA (3 equiv.)	$AlBr_3$ (1 equiv.)	CH_2Cl-CH_2Cl	0-85	0.5-24	1-17
19	**10** (1 equiv.)	PFA (3 equiv.)	$AlBr_3$ (1 equiv.)	$CHCl_3$	0-50	2-24	1-10[1]
20	**10** (1 equiv.)	PFA (3 equiv.)	$AlBr_3$ (1 equiv.)	CH_2Cl_2	0-30	2-24	0
21	**10** (1 equiv.)	PFA (3 equiv.)	CF_3SO_3H (1 equiv.)	CH_2Cl-CH_2Cl	0-85	0.5-5	15-74
22	**10** (1 equiv.)	PFA (3 equiv.)	CF_3SO_3H (1 equiv.)	$CHCl_3$	0-50	0.5-5	1-17[1]
23	**10** (1 equiv.)	PFA (3 equiv.)	CF_3SO_3H (1 equiv.)	CH_2Cl_2	0-30	0.5-5	0
24	**10** (1 equiv.)	PFA (3 equiv.)	CF_3COOH (1 equiv.)	CH_2Cl-CH_2Cl	0-85	0.5-5	0
25	**10** (1 equiv.)	PFA (3 equiv.)	CF_3COOH (1 equiv.)	$CHCl_3$	0-50	2-24	0
26	**10** (1 equiv.)	PFA (3 equiv.)	CF_3COOH (1 equiv.)	CH_2Cl_2	0-30	2-24	0
27	**10**	Paraldehyde	$BF_3 \times Et_2O$	CH_2Cl-CH_2Cl	0-85	0.5-24	5-10

	(1 equiv.)	(3 equiv.)	(1 equiv.)				
28	**10** (1 equiv.)	Paraldehyde (3 equiv.)	CF_3SO_3H (1 equiv.)	CH_2Cl-CH_2Cl	0-85	0.5-24	3-12

[1] According to data of NMR spectroscopy.

2. Crystal data

Table S2. Crystal data and structure refinement for **6**, **7** and **11**.

Compound	**6**	**7**	**11**
Formula	$C_{129}H_{136}N_2O_{40}S_{10}$	$C_{97}H_{143}N_{11}O_{10}$	$C_{150}H_{127}Cl_3N_{12}O_{30}$
Dcalc./ g cm^{-3}	1.392	1.167	1.082
μ/mm-1	2.315	0.596	1.056
Formula Weight	2674.99	1623.22	2683.98
Colour	clear brown	colourless	yellow
Shape	prism	plate	plate
Size/mm^3	0.27×0.18×0.11	0.15×0.09×0.02	0.42×0.23×0.15
T/*K*	99.9(2)	100.00(10)	99.99(10)
Crystal System	monoclinic	triclinic	triclinic
Space Group	*C*2/*c*	*P*-1	*P*-1
a/*Å*	27.2340(4)	12.4634(4)	19.9245(3)
b/*Å*	17.5786(3)	20.2507(12)	20.8844(3)
c/*Å*	26.8160(5)	20.7444(10)	21.69742(17)
α/°	90	63.291(6)	104.8530(11)
β/°	95.9945(14)	81.416(4)	98.5060(10)
γ/°	90	88.833(4)	104.3794(13)
V/Å^3	12767.6(4)	4618.2(4)	8234.8(2)
Z	4	2	2
Z′	0.5	1	1
Wavelength/ Å	1.54184	1.54184	1.54184
Radiation type	Cu K α	Cu K α	Cu K α
θ_{min}/°	2.997	2.414	2.163
θ_{max}/°	77.501	77.237	71.992
Measured Refl.	66822	63746	265502
Independent Refl.	13185	18772	32032
Reflections with $I > 2(I)$	11003	9154	22857
R_{int}	0.0400	0.1296	0.1000
Parameters	822	1093	1758
Restraints	0	0	63

Largest Peak	0.664	1.041	1.004
Deepest Hole	-0.431	-0.397	-1.328
GooF	1.075	1.023	1.436
wR2 (all data)	0.2288	0.2831	0.3620
wR2	0.2181	0.2235	0.3401
R1 (all data)	0.0778	0.1672	0.1259
R1	0.0706	0.0875	0.1096
CCDC Refcode	2027115	2027117	2027116

3. Figure S26. UV spectra and Bindfit (Fit data to 1:1, 1:2 and 2:1 Host-Guest equilibria)

UV-vis spectra of pillar[5]arene 7 (1×10^{-5} M) at different concentrations of PVTE.

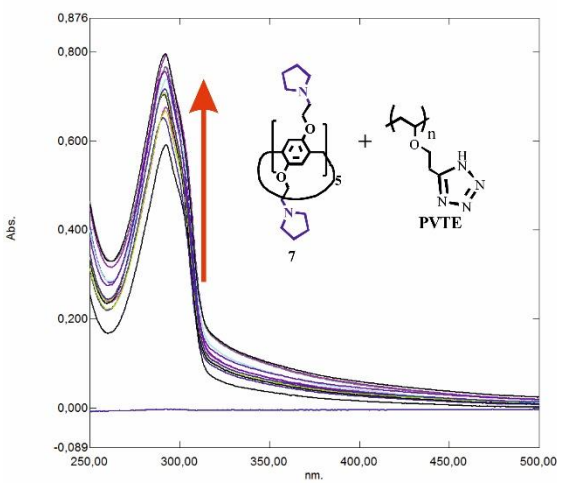

UV-vis spectra of pillar[5]arene 9 (1×10^{-5} M) at different concentrations of PVTE.

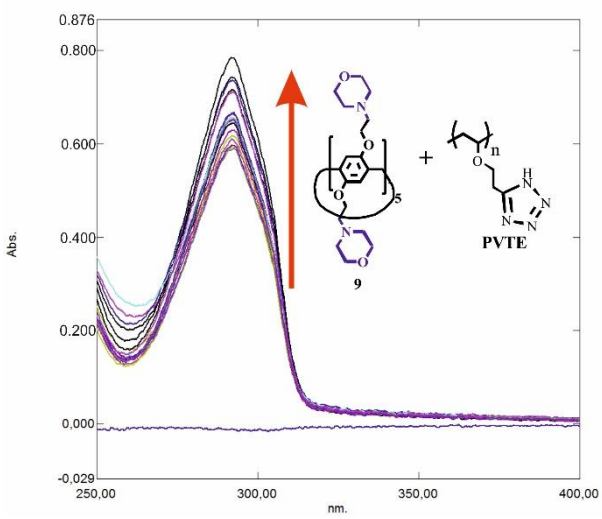

UV-vis spectra of Fluorescein (1×10^{-5} M) at different concentrations of pillar[5]arene 7.

UV-vis spectra of Fluorescein (1×10^{-5} M) at different concentrations of pillar[5]arene 9.

Fluorescence spectra of Fluorescein (1×10^{-5}M) at different concentrations of pillar[5]arene 7.

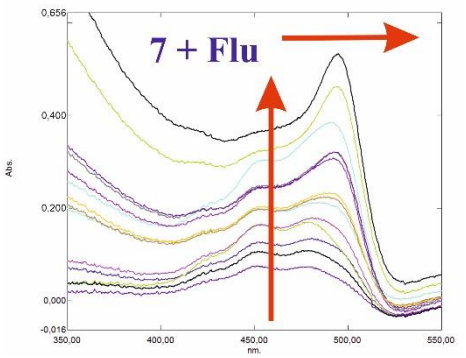
7 + Flu
Abs.
nm.

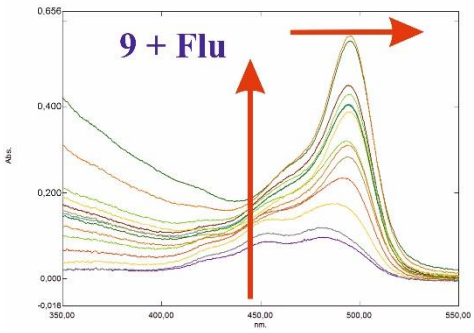
9 + Flu
Abs.
nm.

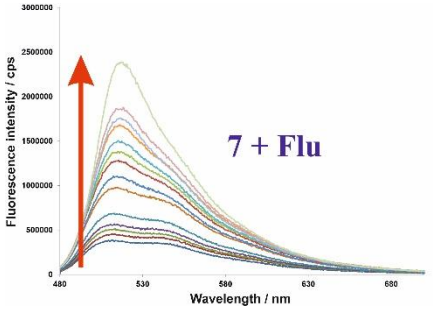
7 + Flu
Fluorescence intensity / cps
Wavelength / nm

Figure S27. Screenshots taken from the summary window of the website supramolecular.org. This screenshots shows the raw data for UV-vis titration of 7 with PVTE, the data fitted to 1:1 binding model (A), 1:2 binding model (B) and 2:1 binding model (C).

(A)

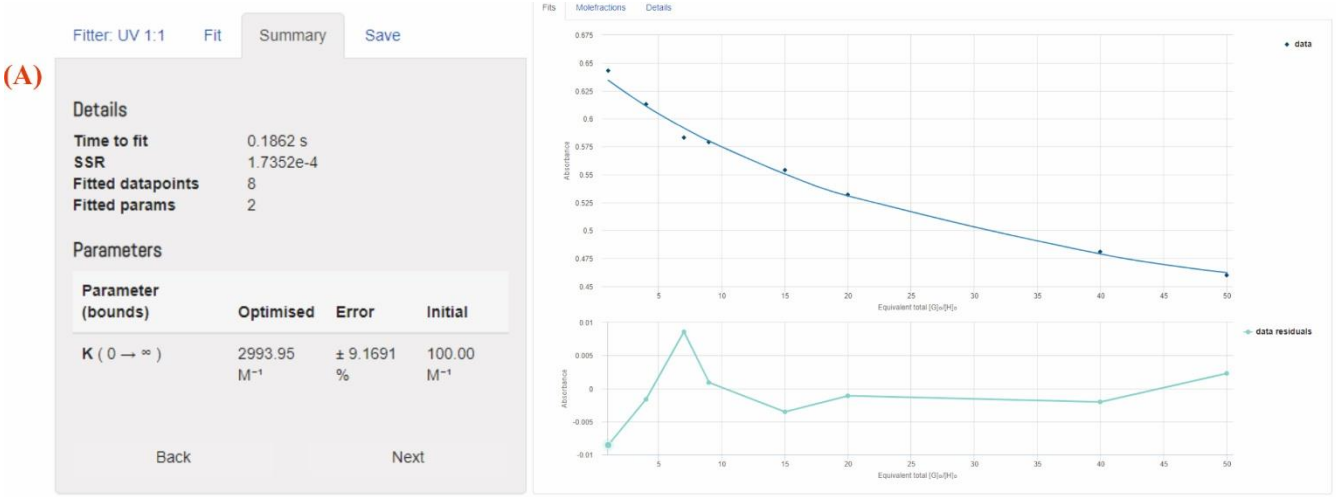

(B)

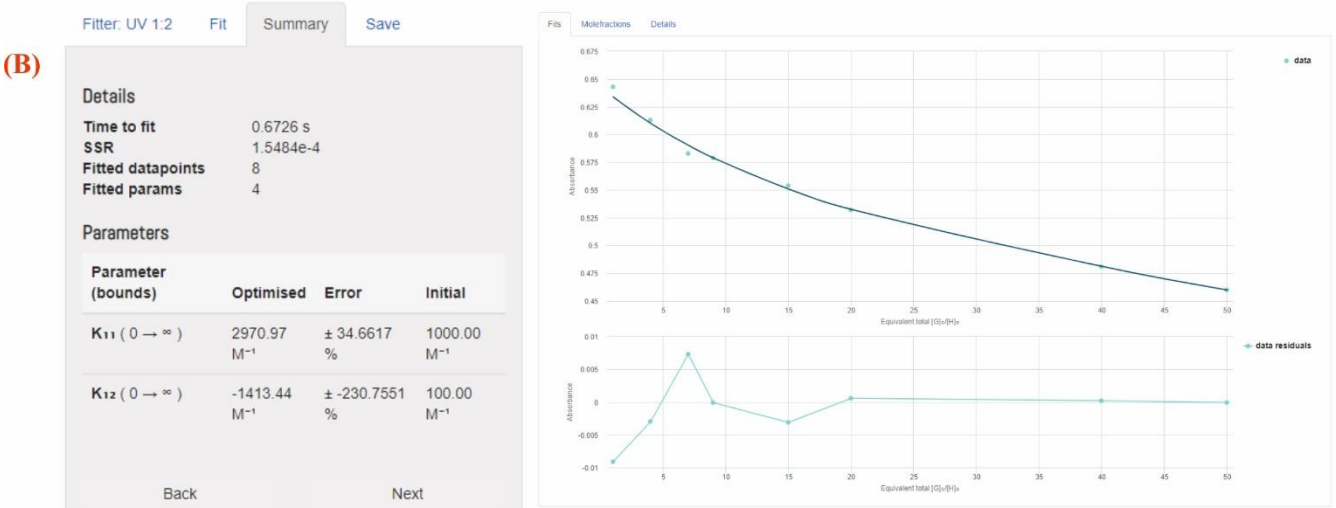

(C)

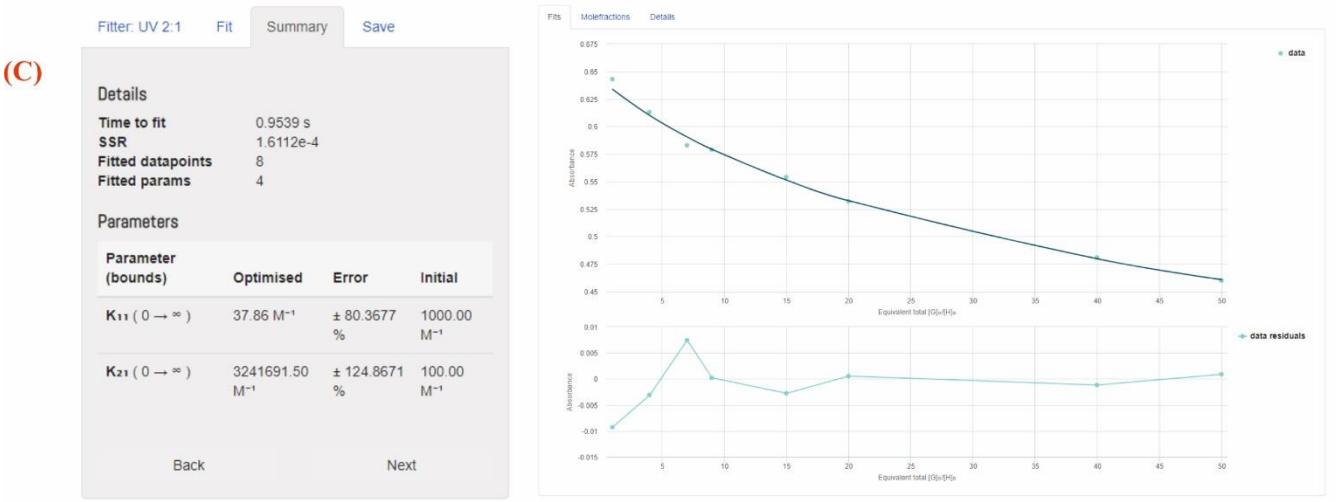

Figure S28. Screenshots taken from the summary window of the website supramolecular.org. This screenshots shows the raw data for UV-vis titration of 9 with PVTE, the data fitted to 1:1 binding model (A), 1:2 binding model (B) and 2:1 binding model (C).

(A)

Fitter: UV 1:1 | Fit | Summary | Save

Details

Time to fit	0.1815 s
SSR	1.8832e-6
Fitted datapoints	6
Fitted params	2

Parameters

Parameter (bounds)	Optimised	Error	Initial
K (0 → ∞)	1898.15 M^{-1}	± 10.7670 %	100.00 M^{-1}

Back Next

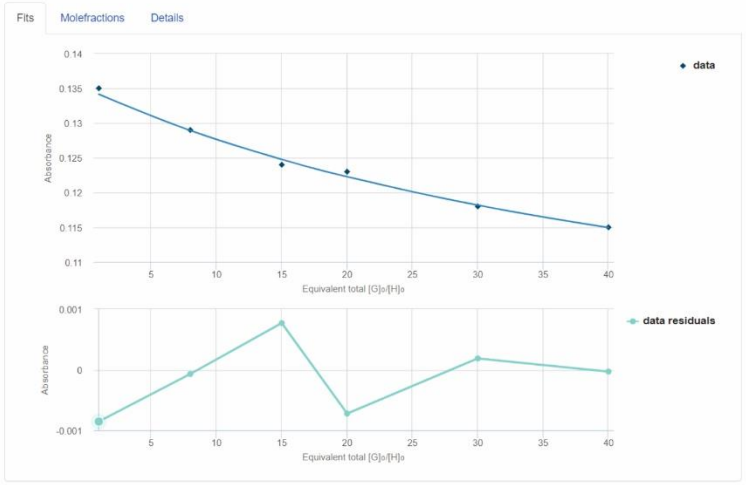

(B)

Fitter: UV 1:2 | Fit | Summary | Save

Details

Time to fit	0.8484 s
SSR	1.2385e-6
Fitted datapoints	6
Fitted params	4

Parameters

Parameter (bounds)	Optimised	Error	Initial
K_{11} (0 → ∞)	152009581692571008.00 M^{-1}	± 1327040882.8891 %	1000. M^{-1}
K_{12} (0 → ∞)	2400.13 M^{-1}	± 25.2300 %	100.0 M^{-1}

Back Next

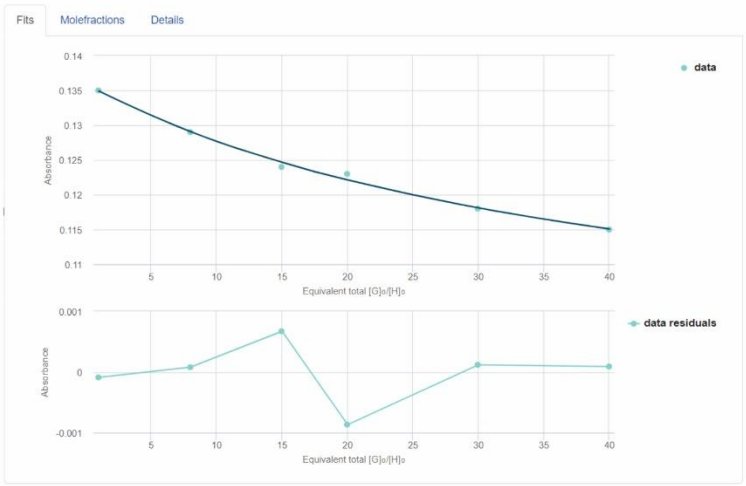

(C)

Fitter: UV 2:1 | Fit | Summary | Save

Details

Time to fit	0.8791 s
SSR	1.0864e-6
Fitted datapoints	6
Fitted params	4

Parameters

Parameter (bounds)	Optimised	Error	Initial
K_{11} (0 → ∞)	3662.85 M^{-1}	± 330.1660 %	1000.00 M^{-1}
K_{21} (0 → ∞)	2338451.31 M^{-1}	± 354.3563 %	100.00 M^{-1}

Back Next

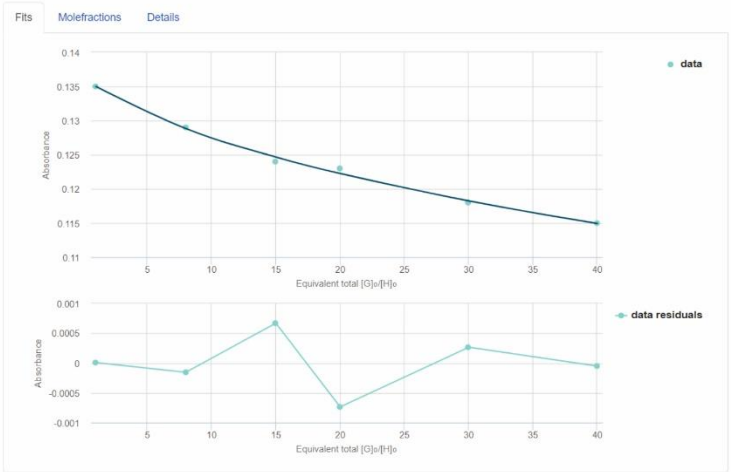

Figure S29. Screenshots taken from the summary window of the website supramolecular.org. This screenshots shows the raw data for UV-vis titration of 7 with Fluorescein, the data fitted to 1:1 binding model (A), 1:2 binding model (B) and 2:1 binding model (C).

Figure S30. Screenshots taken from the summary window of the website supramolecular.org. This screenshots shows the raw data for UV-vis titration of 9 with Fluorescein, the data fitted to 1:1 binding model (A), 1:2 binding model (B) and 2:1 binding model (C).

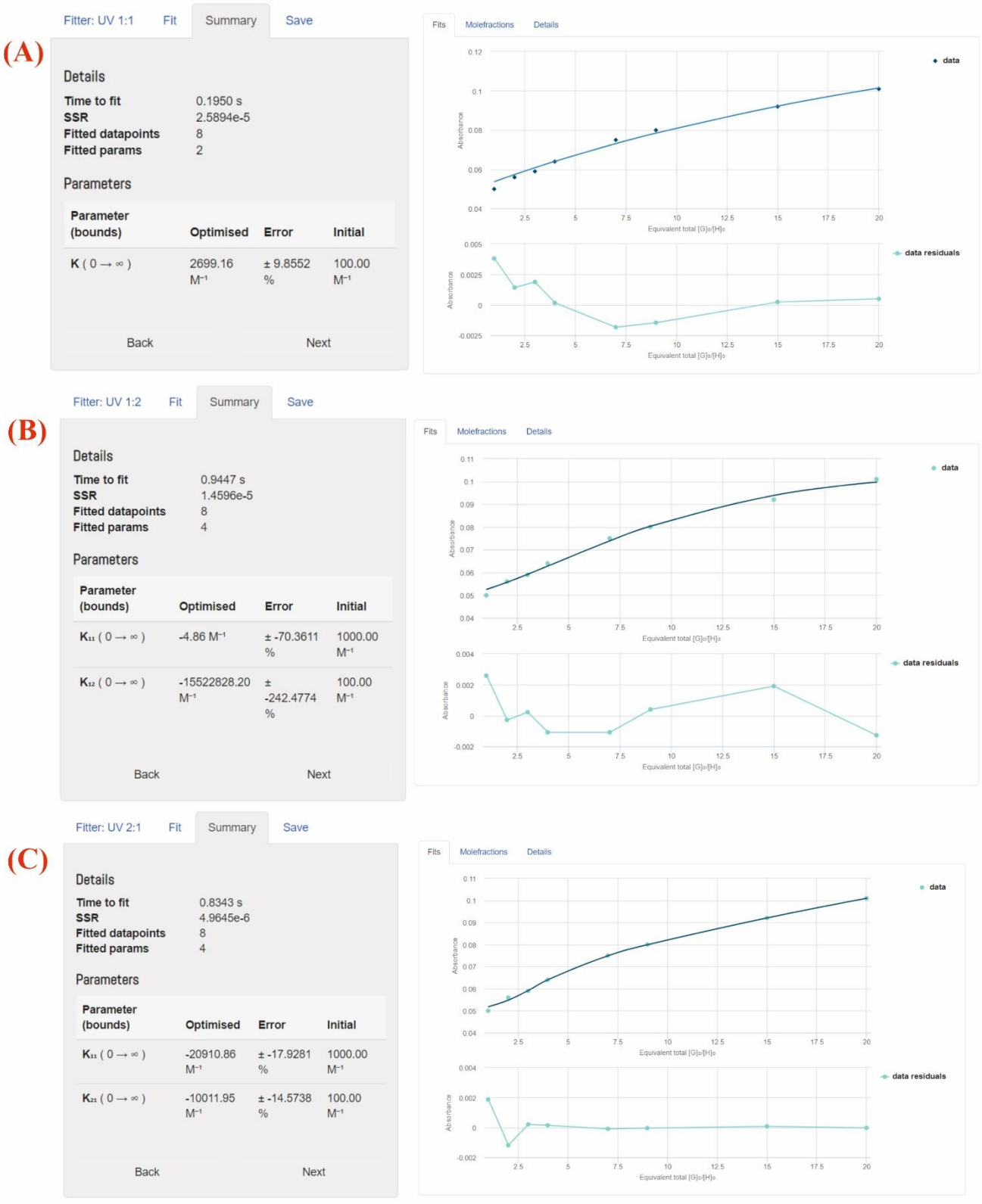

Figure S31. Screenshots taken from the summary window of the website supramolecular.org. This screenshots shows the raw data for fluorescence titration of 7 with Fluorescein, the data fitted to 1:1 binding model (A), 1:2 binding model (B) and 2:1 binding model (C).

(A)

Fitter: UV 1:1 Fit Summary Save

Details

Time to fit	0.1942 s
SSR	13495131713.9540
Fitted datapoints	9
Fitted params	2

Parameters

Parameter (bounds)	Optimised	Error	Initial
K (0 → ∞)	10614.09 M^{-1}	± 10.0111 %	100.00 M^{-1}

Back Next

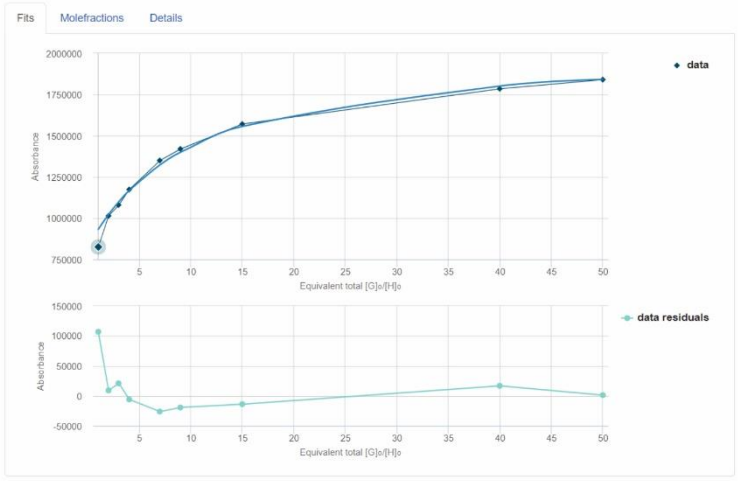

(B)

Fitter: UV 1:2 Fit Summary Save

Details

Time to fit	0.9734 s
SSR	2642467558.3104
Fitted datapoints	9
Fitted params	4

Parameters

Parameter (bounds)	Optimised	Error	Initial
K_{11} (0 → ∞)	38234790356612352.00 M^{-1}	± 67084809.1027 %	1000.00 M^{-1}
K_{12} (0 → ∞)	14527.24 M^{-1}	± 11.7228 %	100.00 M^{-1}

Back Next

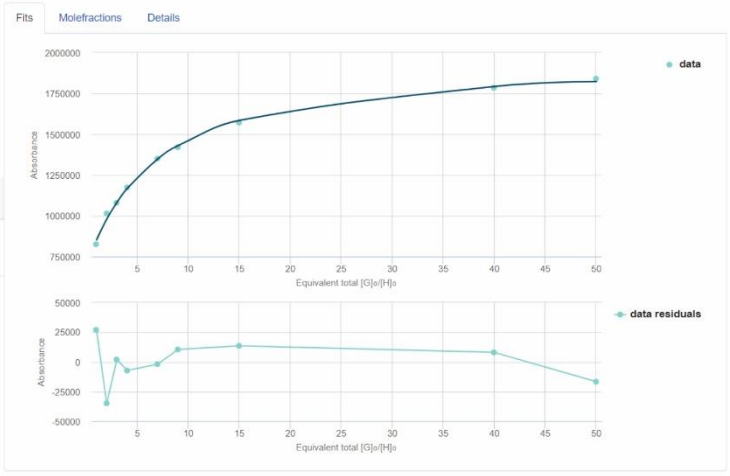

(C)

Fitter: UV 2:1 Fit Summary Save

Details

Time to fit	0.9015 s
SSR	1186825413.6849
Fitted datapoints	9
Fitted params	4

Parameters

Parameter (bounds)	Optimised	Error	Initial
K_{11} (0 → ∞)	227365.07 M^{-1}	± 96.7122 %	1000.00 M^{-1}
K_{21} (0 → ∞)	1005266.52 M^{-1}	± 97.6923 %	100.00 M^{-1}

Back Next

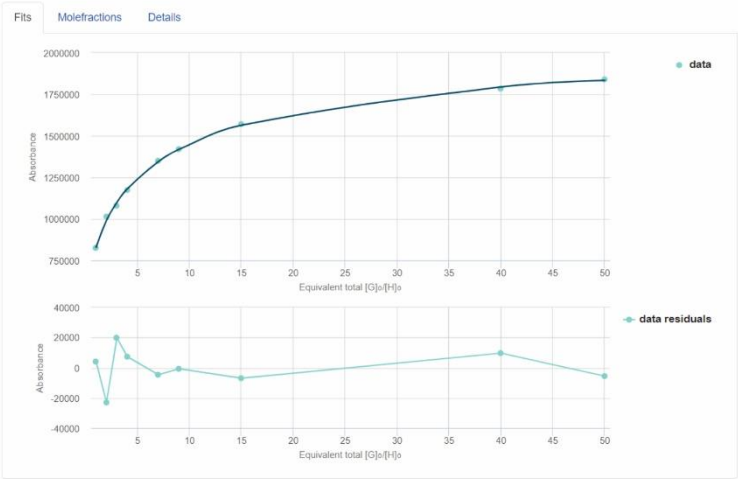

4. Table S3. Dynamic light scattering.

Aggregation of the particles for 7 / Flu and 7 / PVTE in EtOH.

Ratio 7 / Flu	V, μl	C_7, M	C_{Flu}, M	Z average (d) , nm	PDI	ζ- potential, mV
1:0	1000	10^{-3}	0	376.40±34.49	0.42±0.12	-
1:0	1000	10^{-4}	0	406.60±71.45	0.35±0. 10	-
1:0	1000	10^{-5}	0	760.20±111.20	0.44±0.29	-
1:1	1000	10^{-3}	10^{-3}	428.30±8.12	0.36±0.08	3.20±0.10
1:2	1000	10^{-3}	2×10^{-3}	433.90±102.40	0.41 ± 0.02	-
2:1	1000	2×10^{-3}	10^{-3}	305.70±48.18	0.43±0.01	-
1:1	1000	10^{-4}	10^{-4}	336.00±13.60	0.33±0.02	1.40±0.72
1:2	1000	10^{-4}	2×10^{-4}	457.50±149.50	0.47±0.13	-
2:1	1000	2×10^{-4}	10^{-4}	456.80±131.40	0.45±0.11	-
1:1	1000	10^{-5}	10^{-5}	155.40±7.16	0.16±0.02	5.94±0.06
1:2	1000	10^{-5}	2×10^{-5}	225.40±7.12	0.23±0.02	2.50±0.58
2:1	1000	2×10^{-5}	10^{-5}	191.00±25.87	0.26±0.05	2.74±0.14
0:1	1000	0	10^{-3}	460	1	-
0:1	1000	0	10^{-4}	-	-	-
0:1	1000	0	10^{-5}	2328	1	-
7 / PVTE	**V, μl**	**C_7, M**	**C_{PVTE}, M**	**Z average (d) , nm**	**PDI**	**ζ- potential, mV**
50:1	1000	5×10^{-4}	10^{-5}	213.22±4.11	0.31±0.07	-5.44±0.08
10:1	1000	10^{-4}	10^{-5}	116.01±2.26	0.23±0.01	-9.21±0.05
5:1	1000	5×10^{-5}	10^{-5}	198.44±8.10	0.34±0.15	-
2:1	1000	2×10^{-5}	10^{-5}	302.11±1.87	0.35±0.05	-
1:1	1000	10^{-5}	10^{-5}	417.20±11.18	0.39±0.11	-
1:2	1000	10^{-5}	2×10^{-5}	405.54±10.05	0.41±0.17	-
1:5	1000	10^{-5}	5×10^{-5}	440.56±18.16	0.46±0.15	-
1:15	1000	10^{-5}	1.5×10^{-4}	315.20±5.23	0.37±0.28	-
0:1	1000	0	10^{-3}	670.30±456.40	0.60±0.19	-
0:1	1000	0	10^{-4}	108.80±21.02	0.41±0.09	-
0:1	1000	0	10^{-5}	678.00±486.90	0.52±0.17	-

Aggregation of the particles for 9 / Flu and 9 / PVTE in EtOH.

Ratio 9 / Flu	V, μl	C_9, M	C_{Flu}, M	Z average (d), nm	PDI	ζ- potential, mV
1:0	1000	10^{-3}	0	690.10±93.47	0.56±0.34	-
1:0	1000	10^{-4}	0	255.80±96.04	0.58±0. 24	-
1:0	1000	10^{-5}	0	262.30±166.60	0.45±0.14	-
1:1	1000	10^{-3}	10^{-3}	733.70±209.60	0.48±0.37	-
1:2	1000	10^{-3}	2×10^{-3}	1448.00±72.40	0.47 ± 0.12	-
2:1	1000	2×10^{-3}	10^{-3}	760.80±20.55	0.49±0.13	-
1:1	1000	10^{-4}	10^{-4}	876.40±438.80	0.62±0.16	-
1:2	1000	10^{-4}	2×10^{-4}	451.10±221.10	0.44±0.21	-
2:1	1000	2×10^{-4}	10^{-4}	363.20±167.30	0.40±0.14	-
1:1	1000	10^{-5}	10^{-5}	273.50±162.90	0.31±0.16	0.05±0.03
1:2	1000	10^{-5}	2×10^{-5}	309.90±37.24	0.40±0.12	-
2:1	1000	2×10^{-5}	10^{-5}	408.80±176.60	0.45±0.14	-

9 / PVTE	V, μl	C_9, M	C_{PVTE}, M	Z average (d), nm	PDI	ζ- potential, mV
50:1	1000	5×10^{-4}	10^{-5}	312.25±7.12	0.31±0.07	-
10:1	1000	10^{-4}	10^{-5}	125.10±4.15	0.40±0.09	-
5:1	1000	5×10^{-5}	10^{-5}	270.21±5.14	0.38±0.23	-
2:1	1000	2×10^{-5}	10^{-5}	288.60±3.13	0.39±0.10	-
1:1	1000	10^{-5}	10^{-5}	339.45±10.21	0.40±0.08	-
1:2	1000	10^{-5}	2×10^{-5}	550.28±24.35	0.48±0.21	-
1:5	1000	10^{-5}	5×10^{-5}	1120.50±56.40	0.50±0.21	-
1:15	1000	10^{-5}	1.5×10^{-4}	-	-	-

Aggregation of the particles for 7/Flu/PVTE in EtOH.

7/Flu/PVTE	V, μl	C_7, M	C_{Flu}, M	C_{PVTE}, M	Z average (d), nm	PDI	ζ- potential, mV
1:1:0.1	1000	10^{-3}	10^{-3}	10^{-4}	418.24±10.11	0.41±0.12	-
1:1:1	1000	10^{-3}	10^{-3}	10^{-3}	312.15±5.10	0.35±0.14	-
1:1:5	1000	10^{-3}	10^{-3}	5×10^{-3}	214.74±10.08	0.33±0.04	-6.13±0.11
1:1:10	1000	10^{-3}	10^{-3}	10^{-2}	54.11±1.12	0.20±0.04	-11.15±0.10
1:1:0.1	1000	10^{-4}	10^{-4}	10^{-5}	502.11±20.43	0.54±0.21	-
1:1:1	1000	10^{-4}	10^{-4}	10^{-4}	395.00±66.37	0.36±0.04	-8.25±0.54
1:1:5	1000	10^{-4}	10^{-4}	5×10^{-4}	188.23±9.17	0.38±0.09	-9.16±0.36
1:1:10	1000	10^{-4}	10^{-4}	10^{-3}	51.04±2.07	0.21±0.04	-10.79±0.08
1:1:0.1	1000	10^{-5}	10^{-5}	10^{-6}	287.20±34.17	0.32±0.07	-7.14±0.24
1:1:1	1000	10^{-5}	10^{-5}	10^{-5}	114.30±2.10	0.20±0.01	-10.45±0.07
1:1:5	1000	10^{-5}	10^{-5}	5×10^{-3}	102.20±2.24	0.21±0.05	-11.04±0.17
1:1:10	1000	10^{-5}	10^{-5}	10^{-4}	48.02±1.10	0.16±0.01	-12.81±0.04

Aggregation of the particles for 7/Flu/PVTE in H_2O/EtOH (100/1).

7/Flu/PVTE	V_{H2O}, μl	V_{EtOH}, μl	C_7, M	C_{Flu}, M	C_{PVTE}, M	Z average (d), nm	PDI	ζ- potential, mV
1:1:0.1	1000	10	10^{-3}	10^{-3}	10^{-4}	388.58±9.23	0.64±0.25	-
1:1:1	1000	10	10^{-3}	10^{-3}	10^{-3}	324.90±7.80	0.53±0.02	-
1:1:5	1000	10	10^{-3}	10^{-3}	5×10^{-3}	183.45±5.15	0.36±0.09	-9.23±1.47
1:1:10	1000	10	10^{-3}	10^{-3}	10^{-2}	68.26±1.12	0.09±0.01	-34.12±1.94
1:1:0.1	1000	10	10^{-4}	10^{-4}	10^{-5}	1560.40±145.24	1	-
1:1:1	1000	10	10^{-4}	10^{-4}	10^{-4}	417.40±54.39	0.42±0.15	-
1:1:5	1000	10	10^{-4}	10^{-4}	5×10^{-4}	245.36±2.23	0.35±0.04	-9.11±2.13
1:1:10	1000	10	10^{-4}	10^{-4}	10^{-3}	175.00±3.05	0.29±0.01	-26.40±1.45

Aggregation of the particles for 7/Flu/PVTE in buffer (pH 9-2).

7/Flu/PVTE	$V_{buff.}$, μl (pH)	V_{EtOH}, μl	C_7 (EtOH), M	C_{Flu} (EtOH), M	C_{PVTE} (EtOH), M	$Z_{average}$ (d), nm	PDI
1:1:10	1000 (9)	10	10^{-3}	10^{-3}	10^{-2}	82.99±0.47	0.15±0.02
	1000 (7)	10	10^{-3}	10^{-3}	10^{-2}	84.33±0.72	0.12±0.01
	1000 (5)	10	10^{-3}	10^{-3}	10^{-2}	489.33±10.30	0.43±0.15
	1000 (4)	10	10^{-3}	10^{-3}	10^{-2}	688.40±25.69	0.63±0.09
	1000 (2)	10	10^{-3}	10^{-3}	10^{-2}	737.80±45.58	0.55±0.07

Figure S32. Size distribution of the particles by intensity for PVTE (1×10^{-5}M) in ethanol.

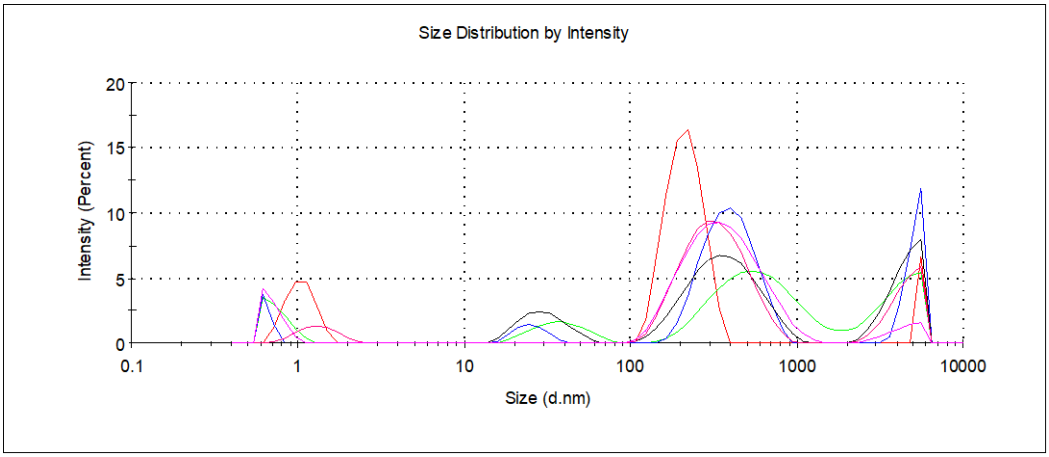

Figure S33. Size distribution of the particles by intensity for 7 (1×10^{-5}M) in ethanol.

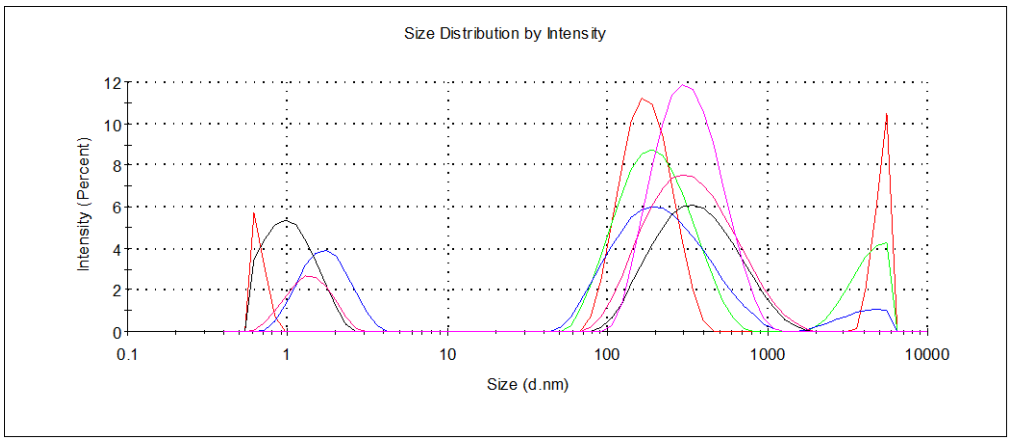

Figure S34. Size distribution of the particles by intensity for 7 (1×10^{-4} M) / PVTE (1×10^{-5} M) (10:1) in ethanol.

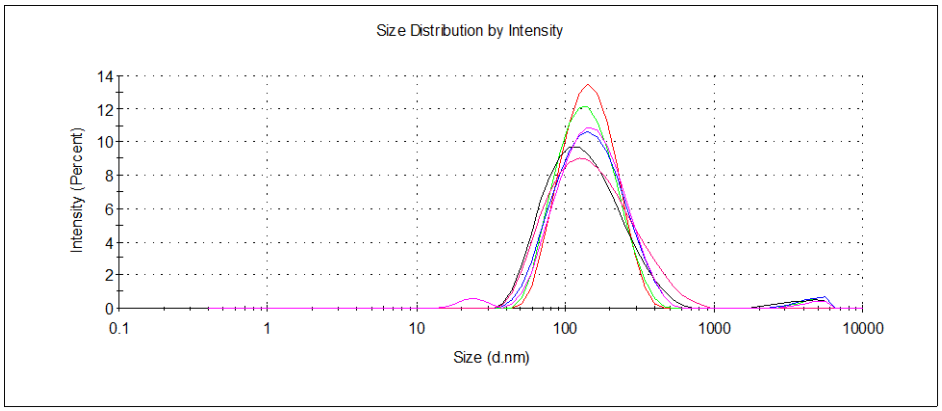

Figure S35. Size distribution of the particles by intensity for **7**/Flu, **7**/Flu/PVTE in ethanol and buffer at different pH.

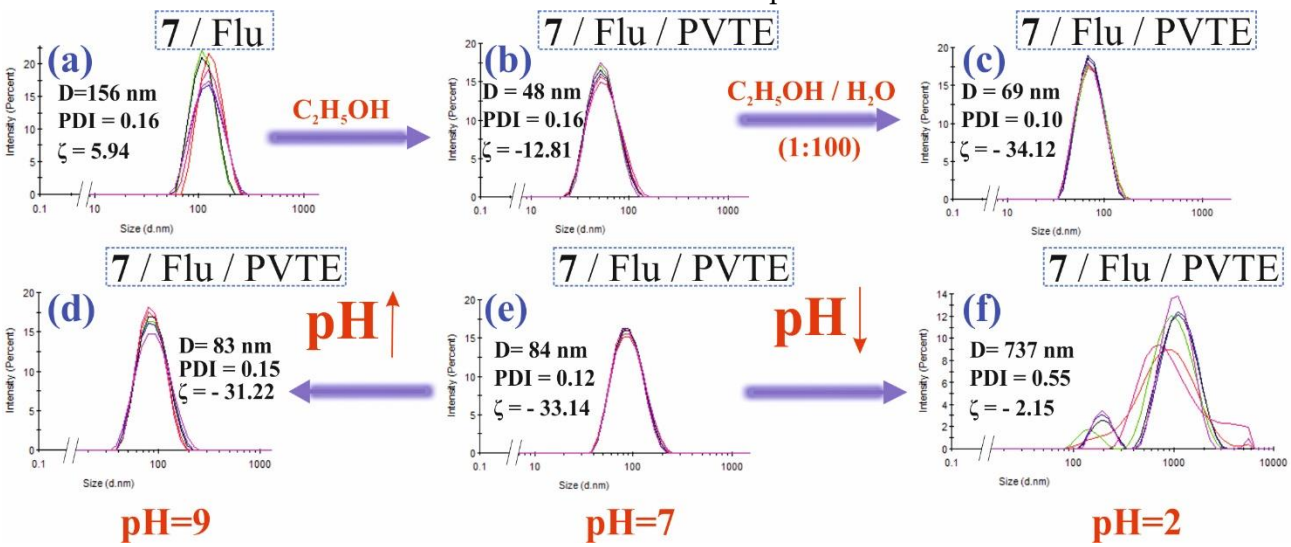

5. Scanning electron microscopy.

Figure S36. SEM image of silicon substrate.

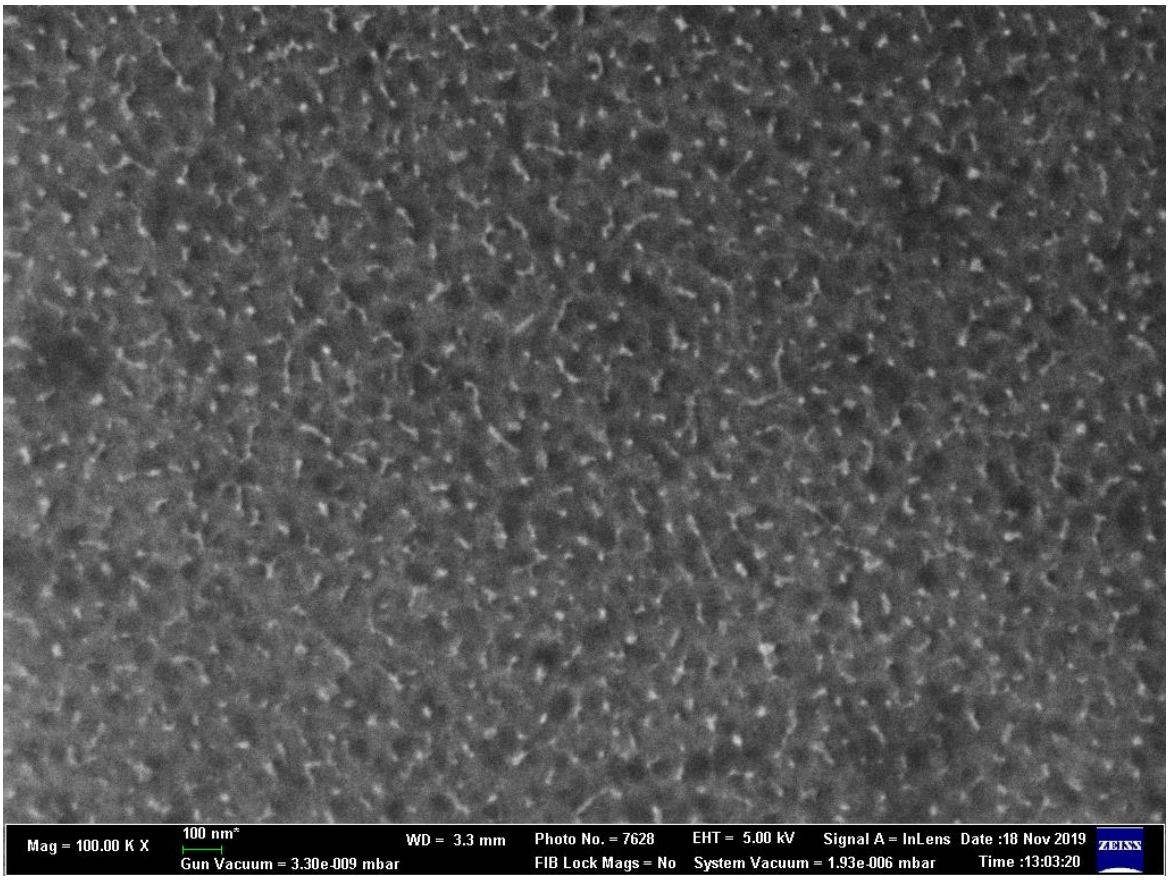

Figure S37. SEM image of 7/Flu/PVTE (1×10^{-5} M) after the solvent (H_2O/EtOH) evaporation.

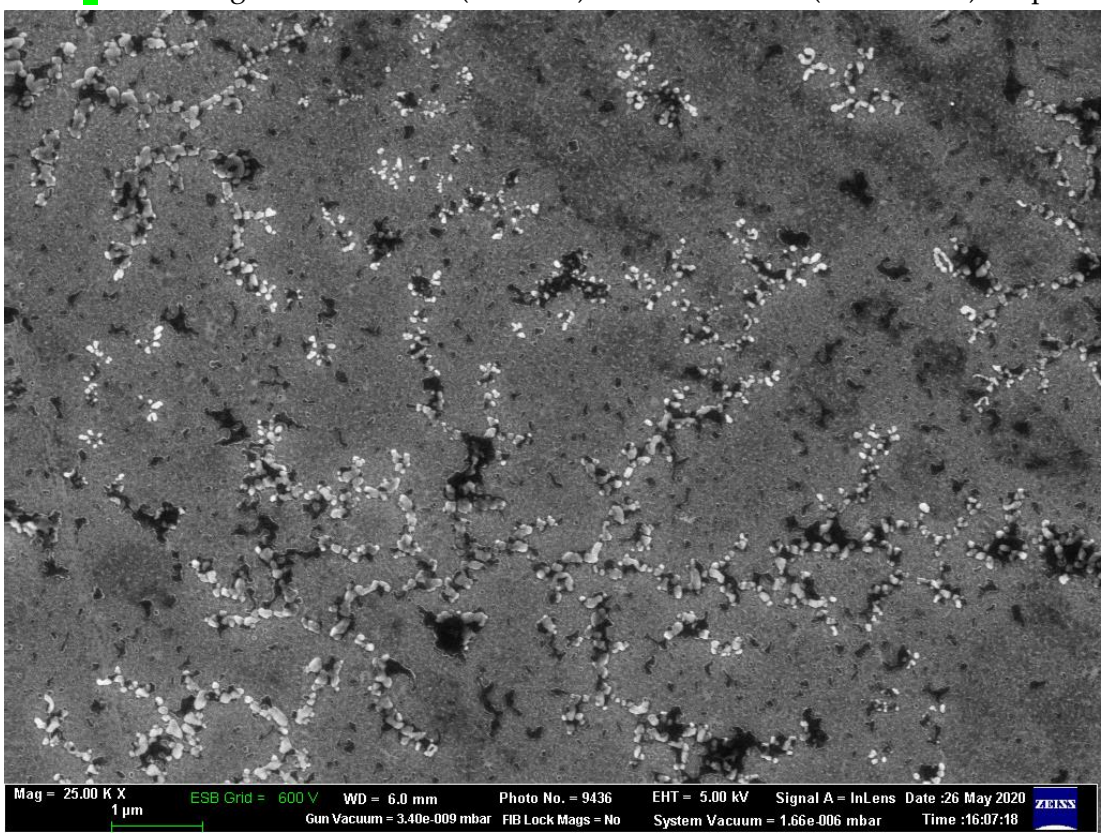

Figure S38. SEM image of 7/Flu/PVTE (1×10^{-5} M) after the solvent (H_2O/EtOH) evaporation.

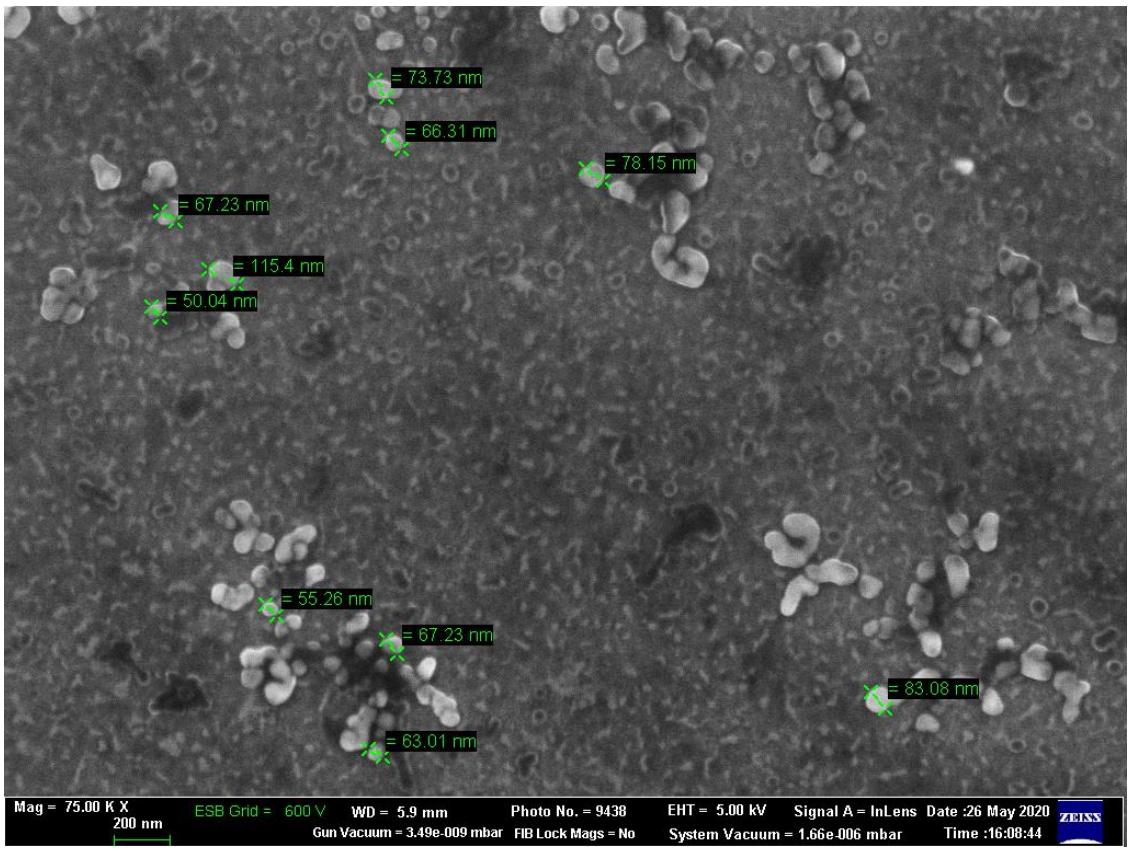

Figure S39. SEM image of 7/Flu/PVTE (1×10^{-5} M) after the solvent (H_2O/EtOH) evaporation.

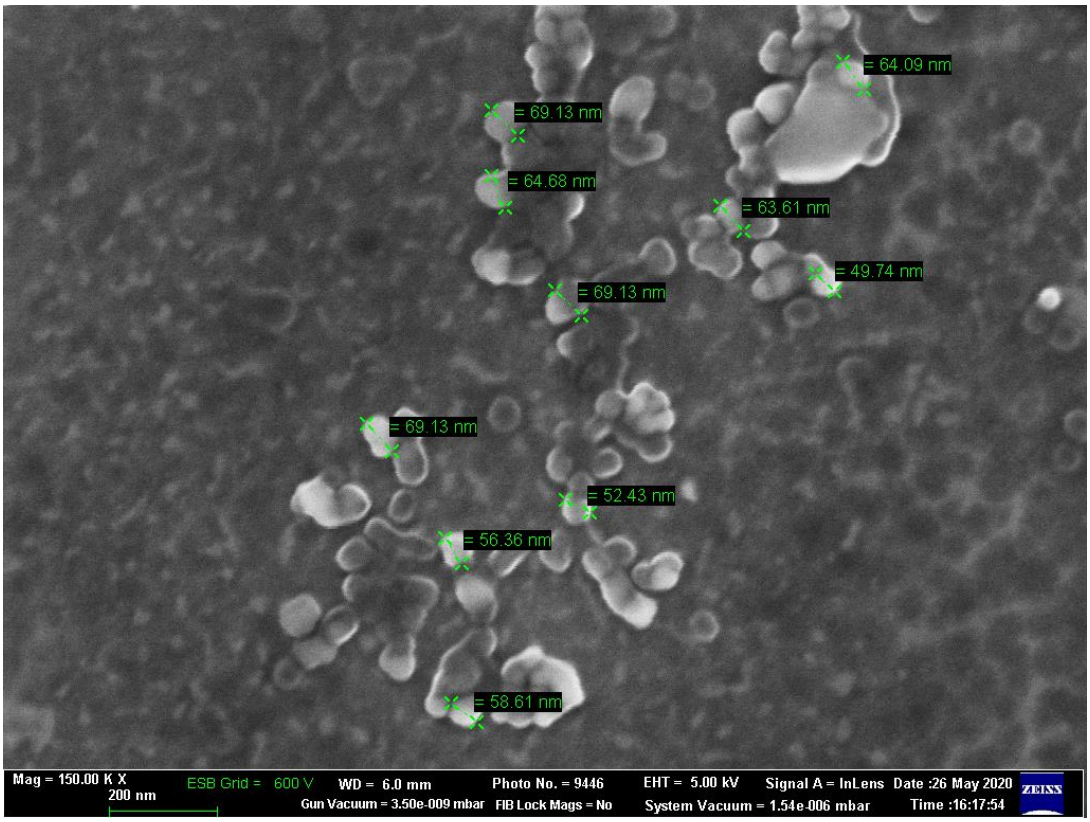

Figure S40. SEM image of 7/Flu (1×10^{-5} M) after the solvent (H_2O/EtOH) evaporation.

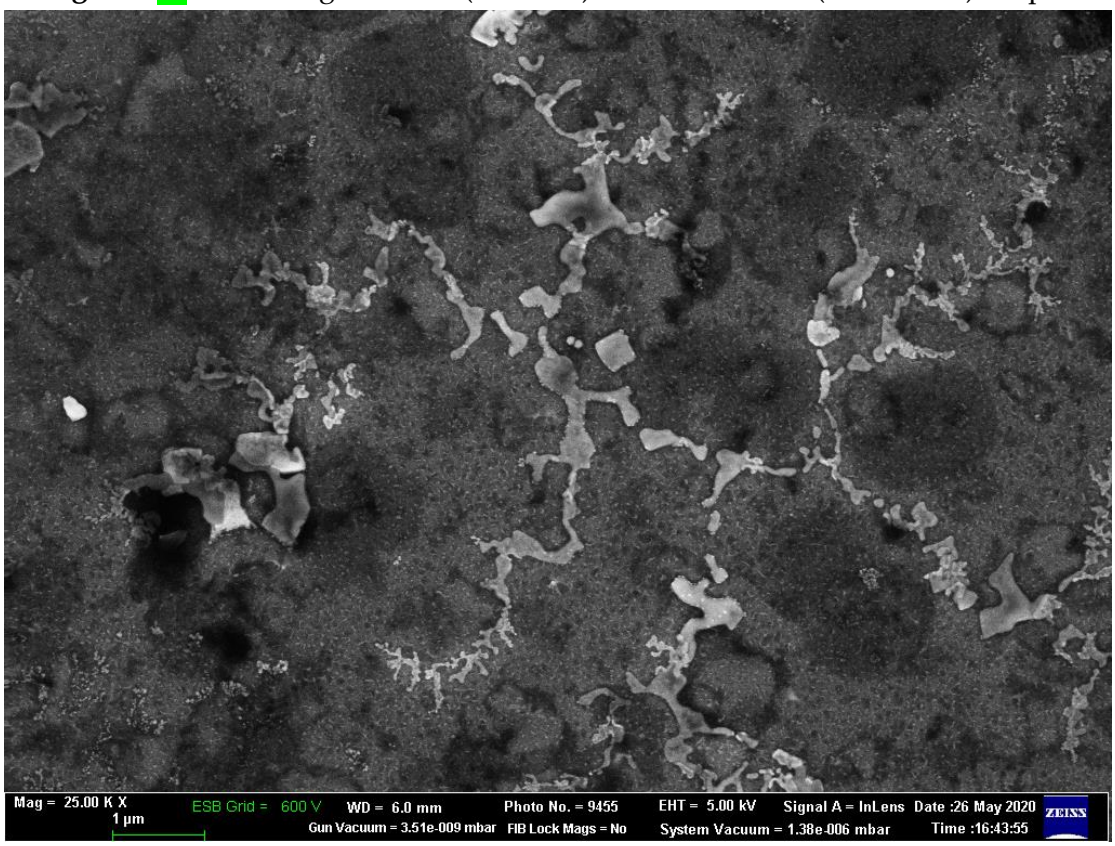

Figure S41. SEM image of PVTE (1×10^{-5} M) after the solvent (H_2O/EtOH) evaporation.

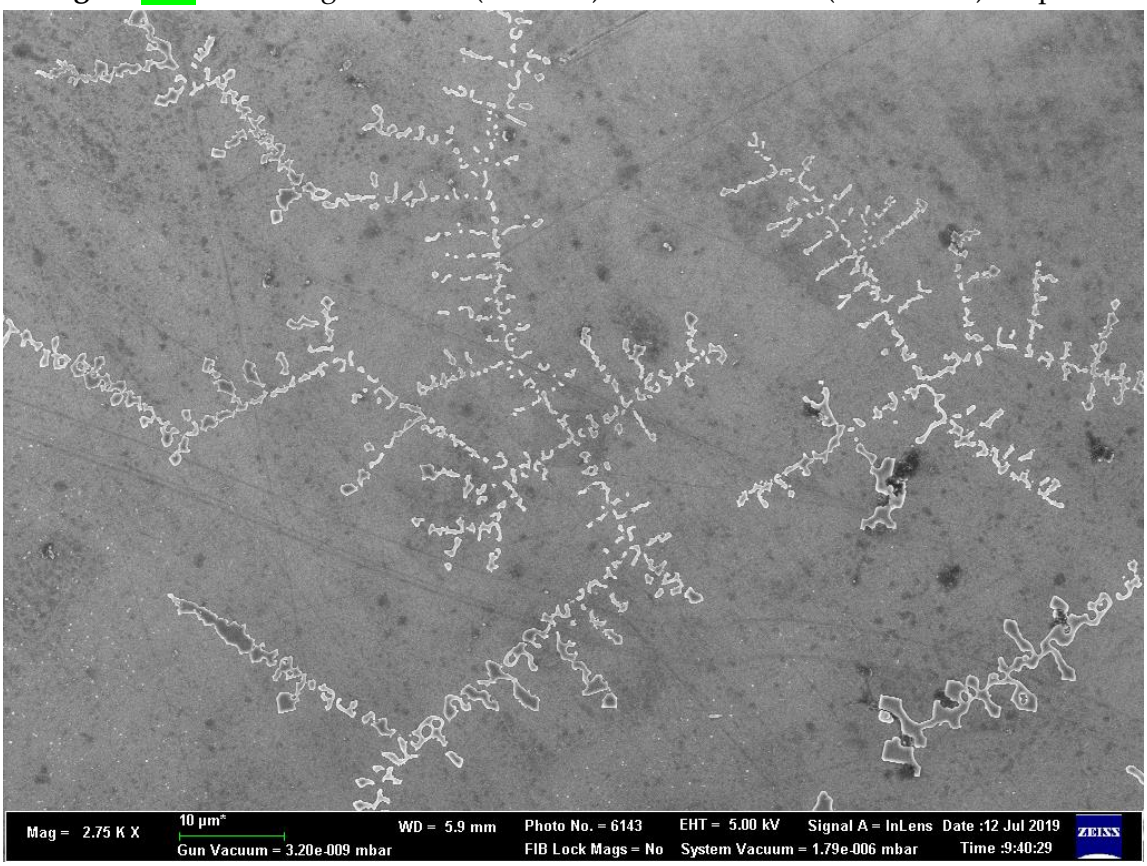

6. Fluorescence spectra

Figure S42. Fluorescence spectra of 7/Flu/PVTE (1×10^{-5}M) in buffer at different pH (9-2).